



TURK GEO

TURKISH JOURNAL OF GEOSCIENCES

g/KUP '4939/98; 8

OPEN ACCESS



dergipark.org.tr/tr/pub/turkgeo
turkgeosciences@gmail.com

VWTMI GQ.'Lwpg4242
Xqno g<3/'Kuwg<3

About The Journal

Turkish Journal of Geosciences is a multi-disciplinary open-access journal aimed to publish peer-reviewed original research and review articles covering all aspects of geosciences. The journal includes a wide scope of information on scientific and technical advances in all areas related to geosciences and indexed in international indices and databases that publish studies on earth sciences.

Aim and Scope

TURKGEO Journal has the following aim and scopes;

Aim of TURKGEO

- TURKGEO aims to promote the theory and practice from the integration of instruments, methodologies, and technologies and their respective uses in the environmental and other natural sciences.
- TURKGEO aims to provide a widely accessible discussion environment that will strengthen and accelerate the exchange of knowledge and experience among scientists, researchers, engineers and other implementers involved in the subject directly or indirectly.

Scope of TURKGEO

- Earth and Environmental Sciences Applications
- Geographic Information Systems
- Remote Sensing
- Photogrammetry
- Geostatistics
- GPS/GNSS
- RADAR/SAR/LIDAR and Laser Scanning
- Spatial Data Infrastructure
- Spatial Decision Support Systems
- Climate Change
- Geology
- Geomorphology
- Hydrogeology
- Geophysics
- Hydrology and Water Resources
- Oceanography

Publishing Frequency

2 issues per year (June-December)

ISSN

2717-7696

WEB

<https://dergipark.org.tr/tr/pub/turkgeo>

Contact

sefa.bilgilioglu@gmail.com / osmanorhan44@gmail.com

EDITOR

Assist. Prof. Dr. Süleyman Sefa BİLGİLİOĞLU

Aksaray University, Faculty of Engineering, Department of Geomatics Engineering /Aksaray/Turkey

ASSOCIATE EDITOR

Assist. Prof. Dr. Osman ORHAN

Mersin University, Institute of Science, Remote Sensing and GIS /Mersin /Turkey

SECTION EDITORS

Assist.Prof. Dr. Bahattin GÜLLÜ, AKSARAY UNIVERSITY
Assist.Prof. Dr. Emine BAŞTÜRK, AKSARAY UNIVERSITY
Dr. Mehmet MESUTOĞLU, KONYA TECHNICAL UNIVERSITY

EDITORIAL BOARD

Prof. Dr. Abdurrahman EYMEN, Erciyes University
Prof. Dr. Alper BABA, Izmir Institute Of Technology
Prof. Dr. C. Serdar BAYARI, Hacettepe University
Prof. Dr. Fatih İŞCAN, Konya Technical University
Prof. Dr. Fevzi KARSLI, Karadeniz Technical University
Prof. Dr. Füsün BALIK ŞANLI, Yıldız Technical University
Prof. Dr. Hakan KARABÖRK, Konya Technical University
Prof. Dr. Hediye ERDOĞAN, Aksaray University
Prof. Dr. Mehmet ÇELİK, Ankara University
Prof. Dr. Murat YAKAR, Mersin University
Prof. Dr. Mustafa YANALAK, ISTANBUL TECHNICAL UNIVERSITY
Prof. Dr. Nebiye MUSAOĞLU, Istanbul Technical University
Prof. Dr. Niyazi ARSLAN, Cukurova University
Prof. Dr. Orhan AKYILMAZ, Istanbul Technical University
Prof. Dr. Reha Metin ALKAN, Istanbul Technical University
Assoc. Prof. Dr. Fatih POYRAZ, Cumhuriyet University
Assoc. Prof. Dr. Hakan YAVAŞOĞLU, Istanbul Technical University
Assoc. Prof. Dr. Himmet KARAMAN, Istanbul Technical University
Assoc. Prof. Dr. Hüseyin KARAKUŞ, Dumlupınar University
Assoc. Prof. Dr. İbrahim TIRYAKIOĞLU, Afyon Kocatepe University
Assoc. Prof. Dr. Mustafa EL-RAWY, Shaqra University
Assoc. Prof. Dr. Serkan DOĞANALP, Konya Technical University
Assoc. Prof. Dr. Tekin SUSAM, Gazi Osman Pasa University
Assoc. Prof. Dr. Uğur AVDAN, Eskisehir Technical University
Assoc. Prof. Dr. Zaide DURAN, Istanbul Technical University
Assist. Prof. Dr. Aydan YAMAN, Aksaray University
Assist. Prof. Dr. Bahattin GÜLLÜ, Aksaray University
Assist. Prof. Dr. Can İBAN, Mersin University
Assist. Prof. Dr. Erkan YILMAZER, Aksaray University
Assist. Prof. Dr. Emine BAŞTÜRK, Aksaray University
Assist. Prof. Dr. Esra GÜRBÜZ, Aksaray University
Assist. Prof. Dr. Kamil KARATAŞ, Aksaray University
Assist. Prof. Dr. Nizar POLAT, Harran University
Assist. Prof. Dr. Özlem GÜLLÜ, Aksaray University
Assist. Prof. Dr. Resul ÇÖMERT, Gumushane University
Assist. Prof. Dr. Sefa YALVAÇ, Gumushane University
Assist. Prof. Dr. Zehra YIGIT AVDAN, Eskisehir Technical University
Dr. Burak Ömer SARAÇOĞLU
Dr. Fabiana CALO, CNR IREA
Dr. Homayoun MOGHIMI, Payame Noor University
Dr. Kaan KALKAN, TUBITAK-UZAY Space Technologies Research Institute
Dr. Syed Mobasher AFTAB, University Of Balochistan

ADVISORY BOARD

Prof. Dr. Bahadır AKTUĞ, Ankara University
Prof. Dr. Dursun Zafer ŞEKER, Istanbul Technical University
Prof. Dr. Hacı Murat YILMAZ, Aksaray University
Prof. Dr. Hatim ELHATİP, Aksaray University
Prof. Dr. Haluk ÖZENER, Bogazici University
Prof. Dr. Mustafa AFŞİN, Aksaray University
Prof. Dr. Mustafa IŞIK, Aksaray University
Prof. Dr. Yusuf Kağan KADIOĞLU, Ankara University

TECHNICAL STAFF

Ahmet Tarık TORUN, Aksaray University
Burhan Baha BİLGİLİOĞLU, Gumushane University
Cemil GEZGİN, Aksaray University
Halil İbrahim GÜNDÜZ, Aksaray University
Ozan ÖZTÜRK, ISTANBUL Technical University
Mustafa Haydar TERZİ, Aksaray University

Contents

Research Articles;

Page	Article Titles and Authors
1-	<i>Geospatial Data Science Response to COVID-19 Crisis and Pandemic Isolation Tracking</i> Muzaffer Can İBAN
8-	<i>The Performance Evaluation of Image Matching Techniques within UAV Images</i> Hasan Bilgehan MAKİNECİ, Hakan KARABÖRK, Akif DURDU
15-	<i>Determining the Effects of the 2020 Elazığ-Sivrice/Turkey (Mw 6.7) Earthquake from the Surrounding CORS-TR GNSS Stations</i> Sefa YALVAÇ
22-	<i>Determining The Forest Fire Risk with Sentinel 2 Images</i> Rutkay ATUN, Kaan KALKAN, Önder GÜRSOY
27-	<i>Comparison of Different Classification Algorithms for The Detection of Changes on Water Bodies; Karakaya Dam Lake</i> Ahmet Tarık TORUN, Halil İbrahim GÜNDÜZ

Geospatial Data Science Response to COVID-19 Crisis and Pandemic Isolation Tracking

Muzaffer Can İban*¹ 

¹ Mersin University, Faculty of Engineering, Department of Geomatics Engineering, Mersin, Turkey

Keywords

COVID-19
Epidemic Spreading
Community Resilience
Pandemic Isolation
Geospatial Information

ABSTRACT

A novel Coronavirus (COVID-19 or SARS-CoV-2) pandemic has become a unique issue topping the global agenda in 2020. Georeferencing any pandemic brings in a spatial extent to monitoring such public health crises. This will be possible only if data patterns about the pandemic cases have practical and biologically relevant value. This article investigates the use of geospatial data science for monitoring the outbreak and reviews the outcomes of the studies carried out. These studies consist of a variety of techniques, such as real-time geospatial databases for pandemic cases, monitoring medical needs, geospatial dashboards, environmental change detection during the pandemic and data collection. Moreover, this study discusses the concept of pandemic isolation tracking and emphasizes its impact during prevention and recovery phases. As a conclusion, the article presents some recommendations and future perspectives for the use of geospatial data science in epidemiological research and community resilience.

1. INTRODUCTION

Geospatial data science plays a vital role to understand, analyse and visualise the spatial distribution of any phenomenon occurring on Earth. Geographic information systems (GIS) are one of the most valuable tools for managing geospatial data flow. Satellite imagery, on the other hand, enables the researchers to monitor land cover and land use to extract highly meaningful geospatial information. Not only crowdsourcing approach using social media and mobile apps, but also the widespread use of smart sensors are modern opportunities for leveraging geospatial big data. Geospatially labelled and instantaneous datasets present effective solutions for global and local difficulties by using big geospatial data analytics methods (VoPham et al., 2018).

By the beginning of 2020, a novel Coronavirus (COVID-19 or SARS-CoV-2) pandemic has become a unique issue topping the global agenda. On March 11, 2020, the World Health Organisation (WHO) announced COVID-19 a pandemic and most countries have preferred to shut down schools and public areas, including travel bans, mass quarantines or nationwide lockdowns (Cohen &

Kupferschmidt, 2020; Hui et al., 2020).

Epidemiology is a branch of science that monitors the distribution of factors and phenomena affecting directly the public health. It tries to establish the relationships between the diseases and their possible pathogenesis. The variety of environmental, social and personal factors which cause an outbreak of a particular disease should also be examined through spatial and temporal data sets (Porta, 2014).

In this context, this review article scrutinises the importance of the geospatial information for the studies of infectious diseases' epidemiology. For this purpose, the article begins with a literature review that identifies the key functions of the geospatial data use and related examples in previous infectious diseases research. Then, it deeply investigates the geospatial data science's responses to COVID-19 crisis, by reviewing the outcomes of the academic and institutional case studies. These studies cover a variety of techniques, such as recording pandemic cases in a real-time geospatial database, monitoring medical needs, establishing local and global geospatial dashboards, monitoring environmental changes during the lockdowns and the collection of pandemic datasets.

* Corresponding Author

*(muzaffericaniban@outlook.com) ORCID ID 0000-0002-3341-1338

Cite this article

Furthermore, this article introduces the pandemic isolation tracking projects that are being implemented across the globe and it presents the Turkish example to discuss data privacy issues. In the conclusion part, the article presents some recommendations and future perspectives for the use of geospatial data science in epidemiologic researches.

2. GEOSPATIAL DATA SCIENCE RESPONSES TO COVID-19

2.1. Mapping the Infectious Diseases

Previous studies have utilised GIS and satellite images to model how the infectious diseases spread, to determine typical environmental factors (e.g. temperature, humidity, flora and fauna) that cause the outbreak, and to identify which communities and human settlements are under the risk of these diseases (Boone, 2000; Brooker & Michael, 2000; Tran et al., 2016). Apart from infectious diseases, in many countries, GIS techniques have been used as a tool to extract geo-relationships between cancer cases and the environment (for Turkish examples, see Colak et al., 2015; Yomralioglu et al., 2009). Furthermore, there have been also several studies for monitoring the infectious diseases in plants (the ones that are consumed by human beings) caused by pathogenic viruses; consequently, it has been possible to map the infected plants and decreased agricultural productivity using geospatial datasets (Gáborjányi et al., 2003).

Infectious diseases have been geo-localised using a variety of geospatial data since John Snow for the first time mapped the London cholera epidemic in 1854. He found out that contaminated water from a street pump had caused the epidemic even though the foul air had been considered to be the reason (Bynum, 2013).

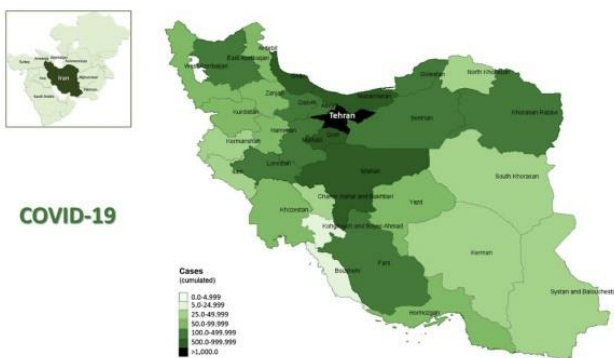


Figure 1. An example from Iran: Mapping cases at province level (Arab-Mazar et al., 2020)

2019-20 Coronavirus pandemic is also being mapped and analysed at global and local scale with real-time case information (for Iranian case, see Figure 1) (Arab-Mazar et al., 2020; Fanelli & Piazza, 2020). While the number of infected people

increases, their travel stories and close contact with other people are being recorded in many countries. Such a record inventory is helpful to decrease the spread of the pandemic and to implement the preventive measures.

2.2. Recording COVID-19 Cases in a Real-time Geospatial Database

A recent study from China, published in *Nature's Scientific Data* journal, shows how real-time infection cases are recorded in a geospatial database, especially in Wuhan City where the virus was first identified. This study presents a geospatial database which contains real-time data sets such as hospital, the date and time when the tests resulted positive and the treatment started, age and gender, observed symptoms, the travel story of the infected individuals. The attention-grabbing aspect of this study is that all recorded cases are geo-coded precisely at the district or even building scale. Such a precise geospatial database has been converted into an automatically-updated interactive web application using Mapbox open-source platform and JavaScript codes. Afterwards, the data sources of other countries (e.g. Western Europe, the United States, Iran and Japan), which record their infection cases at local levels, have been added to [this geospatial database](#); therefore, an [open-source global data visualisation tool](#) (Figure 2) has become available (Xu, Gutierrez, et al., 2020; Xu, Kraemer, et al., 2020).

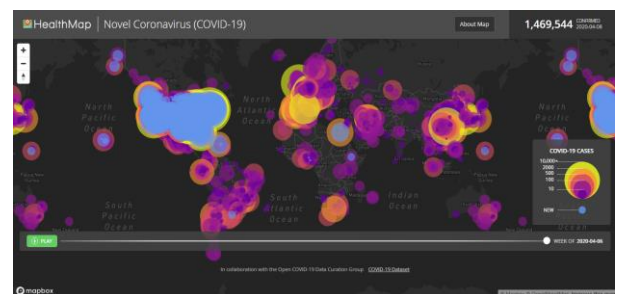


Figure 2. Global COVID-19 Map (Xu, Kraemer, et al., 2020)

The most notable and cited example of a global pandemic map is the interactive web-based dashboard (Figure 3) developed by John Hopkins University Centre for Systems Science and Engineering. The details about this dashboard were published in *The Lancet Infectious Diseases*. Collected data is freely available in their GitHub repository. To track the progression of the pandemic, there have been dozens of similar dashboards at country scale supported by ESRI's ArcGIS Atlas of the World (Dong et al., 2020).

By these dashboards, the users can click on any location and a pop-up displays reported cases in that location. There are several boxes on the right side of the dashboards summarising the total deaths

and recoveries as well as country-by-country details. The data is symbolised as graduated circles, whose size corresponds to the total number of confirmed cases at that location.

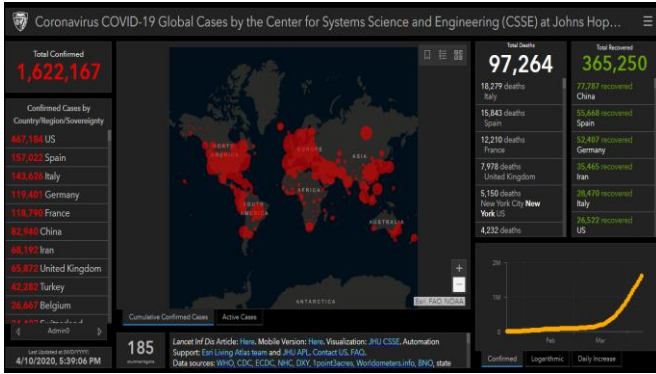


Figure 3. The interactive web-based dashboard (Dong et al., 2020)

2.3. Monitoring Risky Zones and Medical Supplies

Another study from China, published in *Geography and Sustainability*, summarises the short-term gains of big geospatial data management in the context of the fight against a pandemic. Open geospatial data management enables to monitor the contagiousness of the virus throughout the country, from the first case until the latest identified cases. This helps to determine the corridors where the virus travels and to delineate buffer zones depending on the risk density. By mapping the risky areas (see Figure 4), preventive measures can be implemented in those affected areas.

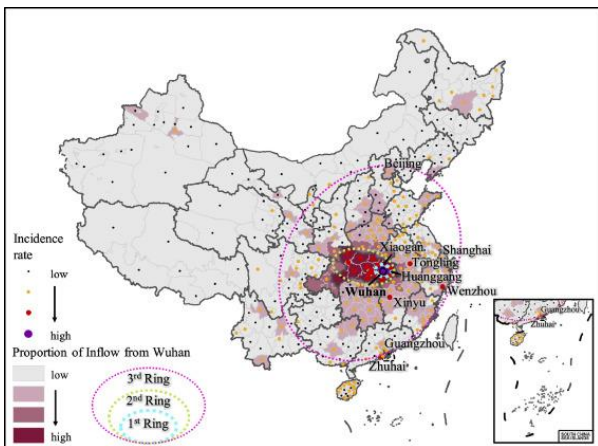


Figure 4. Determining the Risky Areas in China (Zhou et al., 2020)

Another gain is that such a big geospatial inventory can collect the instantaneous medical needs of the institutions across the country (Figure 5). Such a data flow should be open to the public in order to make the medical industry fulfil the needs of the doctors immediately. Manufacturing companies, public health institutions and logistic

chains will be able to monitor the need and transport of medical supplies more straightforwardly, as proven by the study (Zhou et al., 2020). Another example of accelerating medical supply and patient transportation is the Copernicus satellite imagery usage of European Commission (EC). The EC was able to speed up the customs procedures at member states' borders to let the vehicles pass through the long queues rapidly.

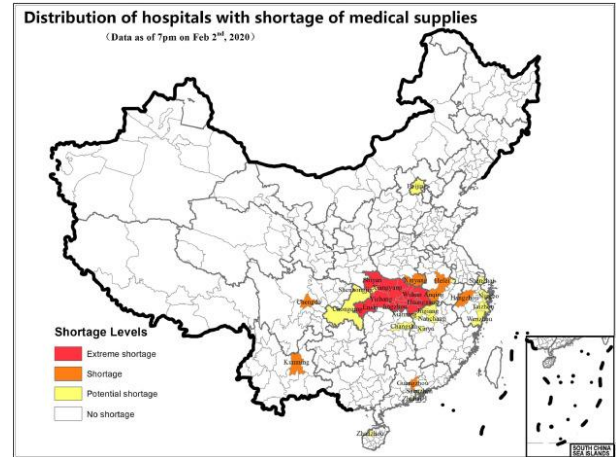


Figure 5. Distribution of Medical Supply Needs (Zhou et al., 2020)

2.4. Collection of Pandemic Datasets

Governmental institutions every day publish COVID-19 datasets for identified cases, recovered and dead patients. However, datasets mostly are not published in a machine-readable format (such as .xls or .csv files and JSON file format). For instance, the Italian Civil Protection publishes their daily reports with PDF format or scanned files on their website (Borruso, 2020). Turkish Health Ministry also has not published any machine-readable dataset, instead, it uses pdf files and screenshots maps (Turkish Ministry of Health, 2020). To cope with such a big non-machine-readable data flow, volunteer data analysts rewrite these data and publish them in personal [GitHub repositories](#), [Kaggle](#) or many other data warehouses (Borruso, 2020).

Worldometers (an international team of developers) every day collects the published data of each country (Figure 6) and researchers can freely extract this tabular dataset via web requests (Worldometer, 2020). The positive cases in Turkey are being mapped at street level through a mobile application (named as *Hayat Eve Sığar*) by the Ministry of Health; however, these datasets are neither downloadable nor machine-readable (Figure 7). The aim of this application is to warn the users about the risks in their territory. Practically, there is not an open-source, vector-format GIS for geo-localising COVID-19 cases in Turkey.

Country/Other	Total Cases	New Cases	Total Deaths	New Deaths	Total Recovered	Active Cases	Serious/Critical	Total Cases/1M pop	Deaths/1M pop	Total Tests	Tests/1M pop
World	1,697,356	+93,602	102,667	+6,983	376,106	1,218,583	49,830	218	13.2		
USA	501,880	+33,314	18,699	+2,017	27,239	455,942	10,916	1,516	56	2,538,789	7,670
Spain	158,273	+5,051	16,081	+634	55,668	86,524	7,371	3,385	344	355,000	7,593
Italy	147,577	+3,951	18,849	+570	30,455	98,273	3,497	2,441	312	906,864	14,999
France	124,869	+7,120	13,197	+987	24,932	86,740	7,004	1,913	202	333,807	5,114
Germany	122,171	+3,936	2,767	+160	53,913	65,491	4,895	1,458	33	1,317,887	15,730
China	81,907		3,336		77,455	1,116	144	57	2		
UK	73,758	+8,681	8,958	+980	344	64,456	1,559	1,086	132	316,836	4,667
Iran	68,192	+1,972	4,232	+122	35,465	28,495	3,969	812	50	242,568	2,888
Turkey	47,029	+4,747	1,006	+98	2,423	43,600	1,667	558	12	307,210	3,643

Figure 6. A part of Worldometer’s case report (Worldometer, 2020)

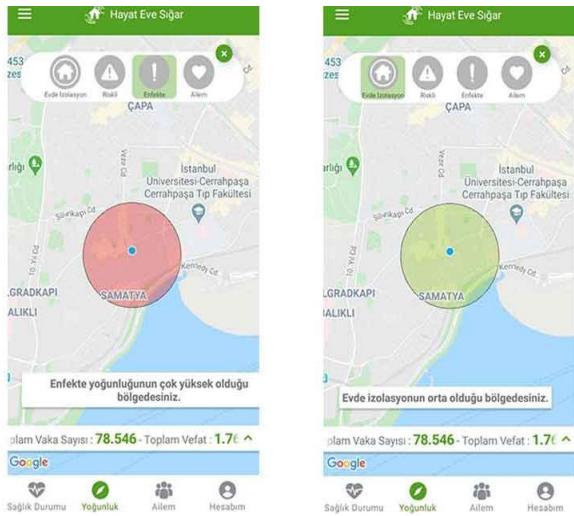


Figure 7. Hayat Eve Sığar Mobile App by Turkish Ministry of Health

2.5. Environmental Monitoring during a Pandemic

NASA and European Space Agency (ESA) pollution monitoring satellites (TROPOMI sensor on ESA’s Sentinel-5 and OMI sensor on NASA’s Aura) sensed a remarkable decline in nitrogen dioxide (NO₂) over China (Figure 8). This situation proves an economic slowdown after the outbreak of COVID-19. NASA scientists stated that NO₂ levels declined firstly in Wuhan area, then this phenomenon spread across all China, due to the fact that millions of people have been in quarantine (ESA, 2020; NASA Earth Observatory, 2020).

The same situation happened also in Europe. Scientists from the Royal Netherlands Meteorological Institute (KNMI) observed both meteorological and TROPOMI data and monitored the significant reduce in NO₂ concentrations over European cities (Figure 9). Such a decrease in pollutant particles in the atmosphere proves the decrease in demand for oil at the beginning of 2020.

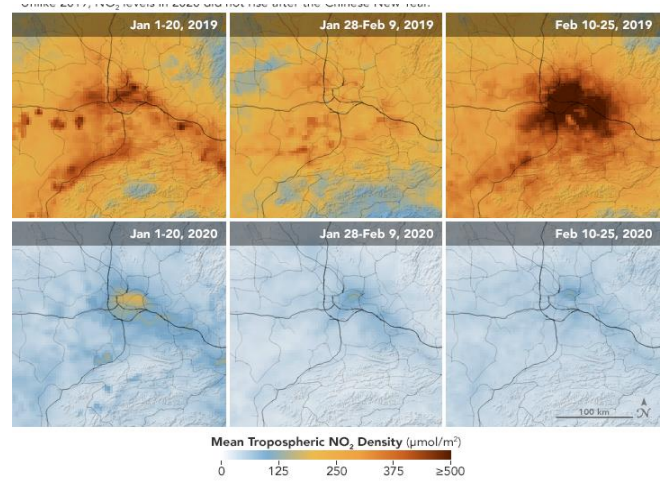


Figure 8. Pollutant Drops in Wuhan in 2019 and 2020 (NASA Earth Observatory, 2020)

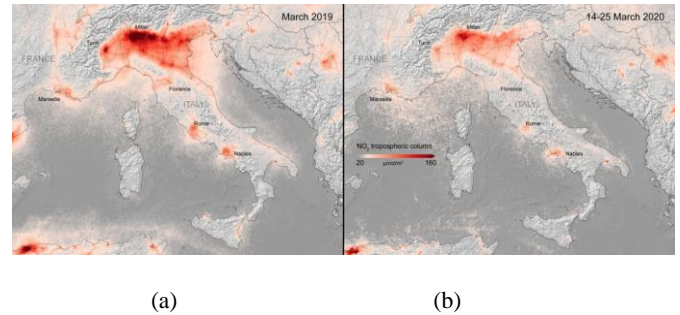


Figure 9. A comparison of NO₂ levels of March 2019 (a) and March 2020 (b) over Italy (ESA, 2020)

3. PANDEMIC ISOLATION TRACKING

Some countries have imposed isolation or curfew measures during the COVID-19 outbreak. The countries, such as South Korea, Singapore, China, Taiwan, Italy, Russia and Israel, have monitored the infected individuals by mobile phone signals and applications. The public services send an SMS message if an infected person leaves their house or anybody that passes nearby a quarantine zone, suggesting them returning to home and isolating themselves. The countries that monitor and map the infected people’s mobility aims at controlling the outbreak spread and implementing strict measures to prevent the close contact; however, it is also commented that such a monitoring process violates the personal freedom and data privacy (The Washington Post, 2020).

3.1. Turkish Pandemic Isolation Project

The Turkish Ministry of Health also announced that they had developed a Pandemic Isolation Tracking Project (in Turkish *Pandemi İzolasyon Takip Projesi*) to slow the spread of COVID-19 outbreak and ensure the isolation of infected

individuals. The Directorate of Communications stated that this practice would be implemented in cooperation with the Ministry of Health, Information Technologies and Communications Authority and all GSM operators. Within the scope of the project, it is planned to monitor whether those who have positive coronavirus tests comply with the isolation and social distancing rules required for the health of themselves, their relatives and the society. The mobility of the quarantined people can be monitored and related analyses can be made to prevent the spread of the pandemic.

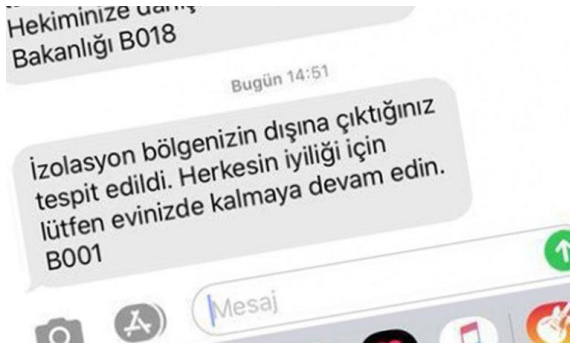


Figure 10. SMS sent to those who leave their home quarantine (Image Credit: *Cumhuriyet Newspaper*)

If the people leave their houses instead of being under home isolation, a warning message (Figure 10) will be sent to their mobile phones. These people will be contacted instantly through automatic call technology and they will be asked to return to where they need to be under isolation. The situation of those who do not comply with the warning and continue with the violation will be shared with the security units, and necessary administrative measures and sanctions will be implemented. The road control police teams also will be able to find out whether the person has violated the isolation by controlling their latest mobility (BBC Turkish, 2020).

3.2. Data Privacy Issues

The Directorate of Communications stressed that the data obtained within the scope of the project will not be used out of pandemic purposes and will be destroyed when the risk of the pandemic ends. Additionally, it was stated that this project does not constitute a violation of Law of Protection of Personal Data (No. 6698) since the third paragraph of Article 6 of the law allows the processing of special personal data without the explicit consent of those concerned, in case there is an exceptional purpose pursued by authorized institutions and organizations for the protection of public health, preventive medicine, medical diagnosis, treatment and care services (BBC Turkish, 2020).

4. RECOMMENDATIONS AND CONCLUSIONS

This review article sums up the geospatial data science responses to the COVID-19 crisis by underlining key outcomes of several academic and institutional initiatives. On the other hand, it identifies the pandemic isolation tracking projects, giving the Turkish example, and underpins the data privacy issues.

Georeferencing any pandemic brings in a spatial extent to monitoring such public health crises. This will be possible only if data patterns about the pandemic cases have practical and biologically relevant value. Moreover, the case studies cited in this review article are good examples and evidence for the importance of determining epidemic trajectories, which require geospatial data sources. The countries should record all COVID-19 cases at a scale as precise as possible (the district, street, even building level) and store them in a geospatial database. These datasets should be opened to at least researchers, national scientific committees, private sector stakeholders (in consulting), local administrations and municipalities that are obliged to implement the preventive measures. If the central administration of countries do not prefer to open such data freely to the public, they need to set up a secure intranet web among these responsible stakeholders. The case studies from China obviously remark that the preventive measures can be relaxed or extended by monitoring the risky zones and the corridors of contagiousness.

The countries need to set up some sort of web applications to fulfil medical doctors' immediate needs. A front-end application with a geospatial dataset, where the medical doctors can insert their supply needs, will be a useful tool to implement immediate actions to supply these medical needs. The ministries will also be able to switch medical supplies between hospitals if one of them needs more than the others.

The literature review shows that tracking pandemic isolation is a new and hot topic for the governance and there has not been any scientific research to identify the data privacy issues and to test the reliability and applicability of the tracking process.

Finally, geospatial data scientists and researchers in the digital earth domain should set up the standards of geospatial data related to pandemic during and after this COVID-19 crisis immediately.

REFERENCES

- Arab-Mazar, Z., Sah, R., Rabaan, A. A., Dhama, K., & Rodriguez-Morales, A. J. (2020). Mapping the incidence of the COVID-19 hotspot in Iran - Implications for Travellers. *Travel Medicine and Infectious Disease*, 101630. <https://doi.org/10.1016/j.tmaid.2020.101630>

- BBC Turkish. (2020). *Pandemi İzolasyon Takip Projesi nedir: Covid-19 salgını kapsamında nasıl kullanılacak?* <https://www.bbc.com/turkce/haberler-turkiye-52219300> (Accessed on 10.04.2020)
- Boone, J. (2000). Remote Sensing and Geographic Information Systems: Charting Sin Nombre Virus Infections in Deer Mice. *Emerging Infectious Diseases*, 6(3), 248–258. <https://doi.org/10.3201/eid0603.000304>
- Borruso, A. (2020). Coronavirus, abbiamo trasformato i dati ufficiali in formato machine readable ma chiediamo alle istituzioni di farlo da sole. *OnData*. <http://blog.ondata.it/coronavirus-abbiamo-trasformato-i-dati-ufficiali-in-formato-machine-readable-ma-chiediamo-alle-istituzioni-di-farlo-da-sole/> (Accessed on 10.04.2020)
- Brooker, S., & Michael, E. (2000). *The potential of geographical information systems and remote sensing in the epidemiology and control of human helminth infections* (pp. 245–288). [https://doi.org/10.1016/S0065-308X\(00\)47011-9](https://doi.org/10.1016/S0065-308X(00)47011-9)
- Bynum, W. (2013). In retrospect: On the Mode of Communication of Cholera. *Nature*, 495(7440), 169–170. <https://doi.org/10.1038/495169a>
- Cohen, J., & Kupferschmidt, K. (2020). Strategies shift as coronavirus pandemic looms. *Science*, 367(6481), 962–963. <https://doi.org/10.1126/science.367.6481.962>
- Colak, E. H., Yomralioglu, T., Nisanci, R., Yildirim, V., & Duran, C. (2015). Geostatistical analysis of the relationship between heavy metals in drinking water and cancer incidence in residential areas in the Black Sea region of Turkey. *Journal of Environmental Health*, 77(6), 86–93. <http://www.ncbi.nlm.nih.gov/pubmed/25619041>
- Dong, E., Du, H., & Gardner, L. (2020). An interactive web-based dashboard to track COVID-19 in real time. *The Lancet Infectious Diseases*. [https://doi.org/10.1016/S1473-3099\(20\)30120-1](https://doi.org/10.1016/S1473-3099(20)30120-1)
- ESA. (2020). *Coronavirus lockdown leading to drop in pollution across Europe*. https://www.esa.int/Applications/Observing_the_Earth/Copernicus/Sentinel-5P/Coronavirus_lockdown_leading_to_drop_in_pollution_across_Europe (Accessed on 10.04.2020)
- Fanelli, D., & Piazza, F. (2020). Analysis and forecast of COVID-19 spreading in China, Italy and France. *Chaos, Solitons & Fractals*, 134, 109761. <https://doi.org/10.1016/j.chaos.2020.109761>
- Gáborjányi, R., Pásztor, L., Papp, M., Szabó, J., Mesterházy, Á., Németh, T., & Kőmives, T. (2003). Use of remote sensing to detect virus infected wheat plants in the field. *Cereal Research Communications*, 31(1–2), 113–120. <https://doi.org/10.1007/BF03543257>
- Hui, D. S., I Azhar, E., Madani, T. A., Ntoumi, F., Kock, R., Dar, O., Ippolito, G., Mchugh, T. D., Memish, Z. A., Drosten, C., Zumla, A., & Petersen, E. (2020). The continuing 2019-nCoV epidemic threat of novel coronaviruses to global health — The latest 2019 novel coronavirus outbreak in Wuhan, China. *International Journal of Infectious Diseases*, 91, 264–266. <https://doi.org/10.1016/j.ijid.2020.01.009>
- NASA Earth Observatory. (2020). *Airborne Nitrogen Dioxide Plummets Over China*. <https://earthobservatory.nasa.gov/images/146362/airborne-nitrogen-dioxide-plummets-over-china> (Accessed on 10.04.2020)
- Porta, M. (2014). *A dictionary of epidemiology*. Oxford University Press.
- The Washington Post. (2020). *Location data could help fight covid-19 — but privacy must be protected*. https://www.washingtonpost.com/opinions/global-opinions/location-data-could-help-fight-covid-19--but-privacy-must-be-protected/2020/03/24/64f1eaa0-6d42-11ea-aa80-c2470c6b2034_story.html (Accessed on 10.04.2020)
- Tran, A., Kassié, D., & Herbreteau, V. (2016). Applications of Remote Sensing to the Epidemiology of Infectious Diseases: Some Examples. In *Land Surface Remote Sensing* (pp. 295–315). Elsevier. <https://doi.org/10.1016/B978-1-78548-105-5.50009-8>
- Turkish Ministry of Health. (2020). *Türkiye'deki Güncel Koronavirüs Durumu*. <https://covid19.saglik.gov.tr/> (Accessed on 10.04.2020)
- VoPham, T., Hart, J. E., Laden, F., & Chiang, Y.-Y. (2018). Emerging trends in geospatial artificial intelligence (geoAI): potential

applications for environmental epidemiology.
Environmental Health, 17(1), 40.
<https://doi.org/10.1186/s12940-018-0386-x>

Worldometer. (2020). *COVID-19 Coronavirus Pandemic*.
<https://www.worldometers.info/coronavirus/>
(Accessed on 10.04.2020)

Xu, B., Gutierrez, B., Mearu, S., Sewalk, K., Goodwin, L., Loskill, A., Cohn, E. L., Hswen, Y., Hill, S. C., Cobo, M. M., Zarebski, A. E., Li, S., Wu, C.-H., Hullah, E., Morgan, J. D., Wang, L., O'Brien, K., Scarpino, S. V., Brownstein, J. S., ... Kraemer, M. U. G. (2020). Epidemiological data from the COVID-19 outbreak, real-time case information. *Scientific Data*, 7(1), 106.
<https://doi.org/10.1038/s41597-020-0448-0>

Xu, B., Kraemer, M. U. G., Xu, B., Gutierrez, B., Mearu, S., Sewalk, K., Loskill, A., Wang, L., Cohn, E., Hill, S., Zarebski, A., Li, S., Wu, C.-H., Hullah, E., Morgan, J., Scarpino, S., Brownstein, J., Pybus, O., Pigott, D., & Kraemer, M. (2020). Open access epidemiological data from the COVID-19 outbreak. *The Lancet Infectious Diseases*.
[https://doi.org/10.1016/S1473-3099\(20\)30119-5](https://doi.org/10.1016/S1473-3099(20)30119-5)

Yomralioglu, T., Colak, E. H., & Aydinoglu, A. C. (2009). Geo-relationship between cancer cases and the environment by GIS: a case study of Trabzon in Turkey. *International Journal of Environmental Research and Public Health*, 6(12), 3190–3204.
<https://doi.org/10.3390/ijerph6123190>

Zhou, C., Su, F., Pei, T., Zhang, A., Du, Y., Luo, B., Cao, Z., Wang, J., Yuan, W., Zhu, Y., Song, C., Chen, J., Xu, J., Li, F., Ma, T., Jiang, L., Yan, F., Yi, J., Hu, Y., ... Xiao, H. (2020). COVID-19: Challenges to GIS with Big Data. *Geography and Sustainability*.
<https://doi.org/10.1016/j.geosus.2020.03.005>

The Performance Evaluation of Image Matching Techniques within UAV Images

Hasan Bilgehan Makineci ^{*1}, Hakan Karabörk ¹, Akif Durdu ²

¹Konya Technical University, Faculty of Engineering and Nature Sciences, Department of Geomatics Engineering, Konya, Turkiye

²Konya Technical University, Faculty of Engineering and Nature Sciences, Department of Electrical Electronical Engineering, Konya, Turkiye

Keywords

BRISK
FAST
Image Mosaicing
SURF
UAV

ABSTRACT

It was aimed that the images were acquired with two different types of UAV by feature-based transformation algorithms such as SURF (Speeded Up Robust Features), FAST (Features from Accelerated Segment Test) and BRISK (Binary Robust Invariant Scalable Keypoints) in this study. Images (acquired by both UAV types) grouped by inclination. This classification is based on the wing type of the UAV (Rotary-Wing UAV" and "Fixed-Wing UAV). Images with different characteristics were used to produce mosaics from the algorithms. The first performance preferred a flight height of 30 m (Ground Sample Distance, 0.82 cm/pixel) with the frontal overlap of 80%, and the second performance preferred a flight height of 60 m (GSD, 1.64 cm/pixel) and same overlap. Ten images from both performances were combined in all algorithms. Mismatches have been observed, and the mosaics produced after a very long process are not found satisfactory. According to the results, for rotary-wing UAV (SURF, BRISK and FAST), the algorithm run times were determined as 76.5 minutes, 11 minutes and 1839 minutes. Also, for fixed-wing UAV (SURF, BRISK and FAST), algorithm run times of 238 minutes, 95 minutes and 3350 minutes were determined.

1. INTRODUCTION

The process of producing the orthomosaic image can be done in two different ways: image mosaicing and image stitching. In image stitching, there are small overlaps between images in which the images are put together. In contrast, image mosaic requires extended overlaps and a blending of several images. The feature is a piece of information that has the task of solving computational problems in the process. The features can be specific structures in the image, such as points, edges, or objects (Aslan et. al., 2019). The features may also be the result of a general neighborhood operation or feature detection applied to the image. Features can be divided into two main categories:

- Features found in specific areas of the image, such as mountain peaks, building corners, doors, or interesting shaped points.

Such positioned properties are often referred to as key point properties and are often identified by groups of pixels encircling the point position (Juan and Oubong, 2010).

- Properties that can be matched according to their orientation and appearance within the image are called sharp edges, and they can also be very well representative of the boundaries of objects in overlapping images and the matching lines of images (Durdu, and Korkmaz, 2019).

Key Point is the point that can be interpreted meaningfully in images. The point at which the boundary direction of the object suddenly changes or the intersection point between multiple edge segments (Figure 3).

In this study, it is aimed to acquire the outdoor images proper for the study taken with an unmanned aerial vehicle and mosaicing the images with feature-based transformation algorithms such as SURF

* Corresponding Author

(hbmakineci@ktun.edu.tr) ORCID ID 0000-0003-3627-5826
(hkarabork@ktun.edu.tr) ORCID ID 0000-0001-7387-7004
(adurdu@ktun.edu.tr) ORCID ID 0000-0002-5611-2322

Cite this article

Makineci, H.B., Karabörk, H., Durdu, A. (2020). The Performance Evaluation of Image Matching Techniques within UAV Images. *Turkish Journal of Geosciences*, 1(1), 8-14.

(Speeded Up Robust Features), FAST (Features from Accelerated Segment Test) and BRISK (Binary Robust Invariant Scalable Keypoints) (Cen et al., 2019; Greengard, and Rokhlin, 1986; Rublee et al., 2011).

In this study, the image mosaic theory has been adopted because the overlapping areas of the images are considerably larger than aerial photogrammetry. The comparison of the algorithms researched in the literature such as SURF, FAST and BRISK was performed in the research. The advantages and disadvantages of the algorithms will be investigated by evaluating the results obtained in the study (Tareen et al., 2018). It is aimed to define the last version of this study as the most efficient method of these systems and to find the most appropriate one.

2. MATERIALS AND METHODS

SURF, FAST and BRISK algorithms were used on Unmanned Aerial Vehicle (UAV) images in this research (Makineci, 2016). Mosaics were constructed on two different models of UAV images and process times were recorded. Rotary-wing UAV and fixed-wing UAV are divided from each other as operating principles. While the fixed-wing UAV flies through the sky, the rotary-wing UAV can wait stable in the air. Because they have different positive and negative sides, it is not easy to guess which are required for users.

Speeded Up Robust Features (SURF) granted in 2008. SURF algorithm based on Gaussian scale-space analysis of images. SURF detector relies on the determinant of the Hessian Matrix and it utilises integral images to increase feature-detection speed (Bay et al., 2008; Tareen et al., 2018).

Binary Robust Invariant Scalable Keypoints (BRISK) described in 2011. BRISK detects corners the usage of AGAST algorithm and filters them with FAST Corner score to trying to find maxima inside the scale-space pyramid. The BRISK description is based totally on figuring out the feature course of each characteristic for reaching rotation invariance. To provide illumination invariance outcomes of simple brightness tests also are concatenated, and the descriptor is constructed as a binary string. BRISK features are invariant to scale, rotation and constrained affine changes (Leutenegger et al., 2011; Tareen et al., 2018).

The FAST algorithm is a feature detection algorithm suggested by Rosten and Drummond. FAST algorithm is an advancement of the SUSAN corner extraction algorithm. It maintains the SUSAN algorithm to detect the components of several feature points, and the algorithm has the benefits of high-speed detection and excellent efficiency of feature point detection (Rosten and Tom, 2005; Liang et al., 2012; Wu, 2018)

2.1 Features detection and matching of main components

Detection: Defining feature points

Description: Environmental form around each feature point, light ratios (contrast values), angular status, scale, and in-image rotations, etc. it is defined fixedly (ideally). The identifier is recognized by a vector for each feature point.

Matching: Identifiers are compared between images to find similar features. For two images, a pair in one image $(X_i, Y_i) \leftrightarrow (X'_i, Y'_i)$, (X_i, Y_i) is a feature in another image, (X'_i, Y'_i) is matched if there is a matching feature in both images.

2.2 Points to consider when choosing feature extraction points

The points should have a very well defined position in the image. Despite local distortions in the image, they are fixed as light contract/brightness values, so feature points can be reliably found - with a high probability of repetition.

2.3 The feature identifier

A feature identifier is an algorithm that finds property vectors. Feature identifiers encode different information into a series of numbers and run the information as a kind of numeric "fingerprint" that can be used to differentiate one from another. Ideally, this information should be independent of the image movement. Thus, even if the image is moved in some way, we can find the same feature again. After identifying feature points, an identifier is calculated for each point. Identifiers are divided into two classes:

1. Local Descriptor: An integrated representation of the regional neighborhood relations of a point. This method is very suitable in terms of point matching since a point only deals with the neighborhood and regional relations.

2. Global Descriptor: Global descriptor defines the entire image. It is possible that the change in part of the image will fail, as it will affect the result descriptor, and is usually not very reliable (Zhong, and Yubai, 2019).

2.4 Image matching

Part of several computer visioning applications, such as matching features or image matching in general, image stitching, camera calibration, and object recognition, is the task of detecting that the same object is common to two images. Once the properties and identifiers are specified from two or more images, the next step is to create some preliminary matches between these images (figure 1).

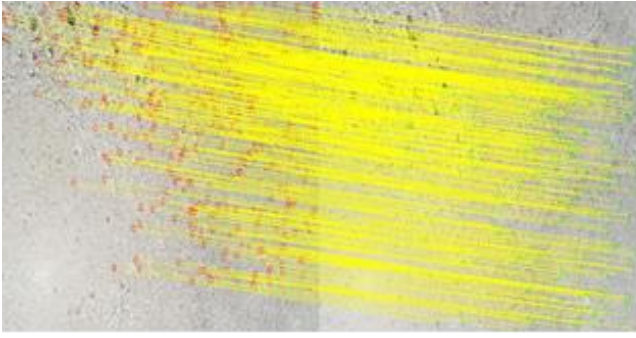


Figure 1. Image matching points

In general, the performance of matching methods based on feature points depends on both the areas of interest of the features and the selection of identifiers of overlapping images. Therefore, detectors and identifiers suitable for the image content should be used in applications. For example, if an image contains bacterial cells, a bubble detector should be used instead of using a corner detector. Feature extraction and matching algorithms processing steps:

- Detect specific key points,
- A region is defined around each key point,
- The defined region is separated and normalized,
- The local identifier is calculated from the normalized region; the defined local identifiers are matched.

2.5 UAVs and cameras

UAV with two different characteristics (according to wing types) was investigated in this study. Fixed-wing UAV (Sense Fly Ebee RTK) and rotary-wing UAV (DJI Phantom 4 Pro) are internationally known industrial brands. The cameras fixed on UAVs are also composite RGB cameras provided by the manufacturer (Figure 2). In particular, the feature that distinguishes these UAVs is their movement in the air. Fixed-wing UAV can fly like a plane and penetrate the wind. In this way, its long battery allows it to operate longer. Rotary-wing UAVs have motor and rotor systems that will remain stationary in the air. That causes more energy consumption. However, it is demanded by the users as it can take off / take off vertically and stand in the air.

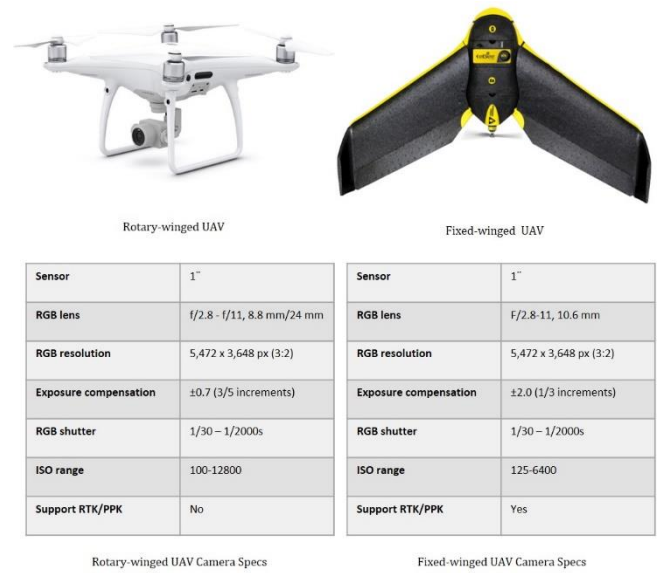


Figure 2. UAVs and camera specs

3. PROCESS OF STUDY

To compare and, if possible, improve the performance of the image matching algorithms, a classification was made based on the slope differences. This classification is based on the selection of images manually. Two types of land structures were identified. The first terrain structure is where the structure of the terrain is considered to be rugged and the slope is observed above 15 ° on average. This land was defined as sloping land. The second type of land is the land structure where the slope does not show very instant changes and the land structure is referred to as flat in the literature and the average slope is below 15 °. This land structure is defined as flat land (Makineci and Karabörk, 2016).

The other compare research of the study is the height and overlay ratio at which the images were taken. Table 1 using all the data in the image matching points were produced and the working principles of the SURF, FAST, BRISK algorithms were investigated. As can be seen from Table 2, which shows the results produced from the images used, different algorithms were able to produce mosaic by showing positive results in different image types. However, results to be classified as positive, negative or results that have been achieved nothing at all (Ruble et al., 2011; Cen et al., 2019; Greengard and Rokhlin, 1986).

Also, in addition, GSD is 2.5 cm/px in fixed wing UAV and 2.2 cm/px in rotary wing UAV for 120 m height. Likewise, for a height of 100 m, the GSD is 2.1 cm/px in fixed wing UAV and 1.85 cm/px in rotary wing UAV.

Table 1. Classification of images used in research

	Fixed-winged UAV Images	Rotary-winged UAV Images
1.Comparision	120m flight height 80 overlap flat area	120m flight height 80 overlap flat area
2.Comparision	120m flight height 80 overlap slope area	120m flight height 80 overlap slope area
	Rotary-winged UAV Images	Rotary-winged UAV Images
3.Comparision	100m flight height 80 overlap flat area	120m flight height 80 overlap flat area
4.Comparision	100m flight height 80 overlap slope area	120m flight height 80 overlap slope area
	Rotary-winged UAV Images	Rotary-winged UAV Images
5.Comparision	100m flight height 80 overlap flat area	100m flight height 70 overlap flat area
6.Comparision	100m flight height 80 overlap slope area	100m flight height 70 overlap slope area
	Rotary-winged UAV Images	Rotary-winged UAV Images
7.Comparision	90m flight height 70 overlap flat area	100m flight height 70 overlap flat area
8.Comparision	90m flight height 70 overlap slope area	100m flight height 70 overlap slope area

Table 2. Mosaic results produced by algorithms according to classes

		<div style="border: 1px solid black; padding: 5px; display: inline-block;"> ROTARY-WING UAV IMAGES </div>								<div style="border: 1px solid black; padding: 5px; display: inline-block;"> FIXED-WING UAV IMAGES </div>	
Algorithms		90m flight height 70 overlap flat area	90m flight height 70 overlap slope area	100m flight height 70 overlap flat area	100m flight height 70 overlap slope area	100m flight height 80 overlap flat area	100m flight height 80 overlap slope area	120m flight height 80 overlap flat area	120m flight height 80 overlap slope area	120m flight height 80 overlap flat area	120m flight height 80 overlap slope area
SURF											
FAST											
BRISK											

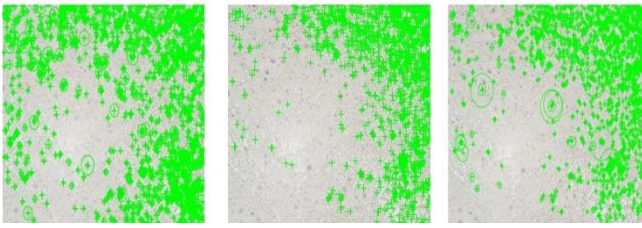


Figure 3. Feature point selection of algorithms

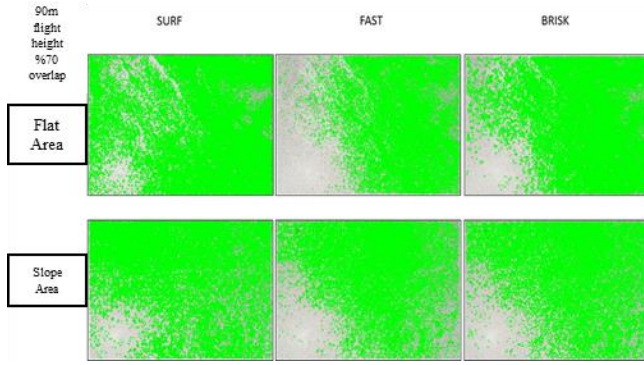


Figure 4. Feature point selection of algorithms

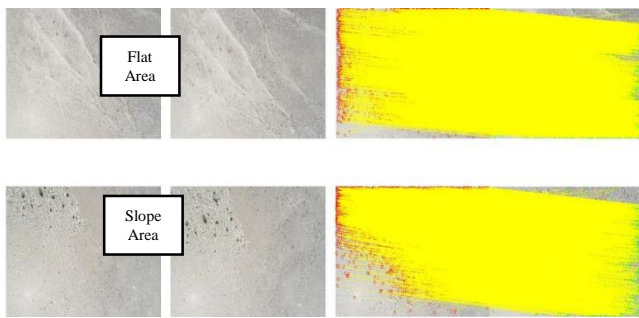


Figure 5. Mosaic extraction from images by matching SURF algorithm feature points

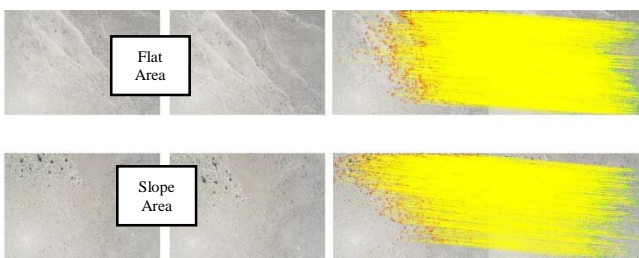


Figure 6. Mosaic extraction from images by matching FAST algorithm feature points

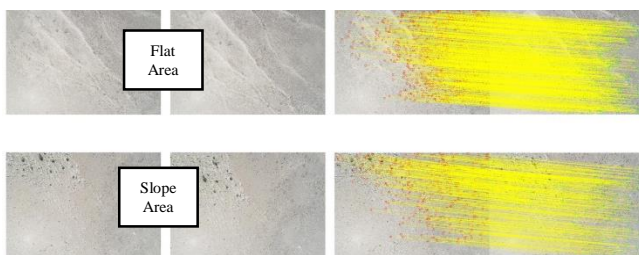


Figure 7. Mosaic extraction from images by matching BRISK algorithm feature points

Figure 3 and Figure 4 show the selection of feature points, Figure 5, Figure 6 and Figure 7 show the mapping of feature points.

Since the mosaic produced using these images did not present positive results, new flights were organised. These new flights were carried out on land more useful for the algorithms to create the mosaic. The result products of this alternative operation are shown in figure 8.

Alternative images were used to produce mosaics from SURF, FAST and BRISK algorithms because the images taken in the field studies did not actually give the expected performance. The flight height of the first project was 30 m (GSD = 0.82 cm / pixel) and the flight height of the second project was 60 m (GSD = 1.64 cm / pixel). 10 images from both projects were combined in all algorithms. The results of these images produced from mosaics are shown in Table 3. Also, Figure 8 shows the mosaics of alternative operations.

The most critical result expected in this study was to determine how the popular FAST, SURF and BRISK algorithms produced in a mosaic from UAV images. For this reason, it was first attempted to produce mosaic using the images (from different heights) acquired with two different types of UAV (Table 2). But in some, the mosaic was never produced. Some of the mosaics were produced for a very long time or were produced inaccurately. Several different searches were made to fix faults. Finally, to a cause of inaccuracy, it was understood that the texture of the land was very similar. For this understanding, new images with different characteristics of the texture were acquired with the rotary-wing UAV. So, it has been tried to determine how much they perform only in producing mosaic. As seen in Figure 7, the mosaics produced are represented as mosaic produced from A 30 m flight altitude images and B 60 m is presented as mosaic produced from flight height images. As and Bs show the mosaics produced from SURF algorithm. The mosaics produced from the Af and Bf FAST algorithm also show the mosaics produced from the Ab and Bb BRISK algorithm.

Table 3. Algorithms and results

Algorithm: SURF	Mosaic Production Time	Mosaic Description
30 m flight height %80 Overlap	76,5 min	As
60 m flight height %80 Overlap	238 min	Bs
Algorithm: BRISK	Mosaic Production Time	Mosaic Description
30 m flight height %80 Overlap	11 min	Ab
60 m flight height %80 Overlap	95 min	Bb
Algorithm: FAST	Mosaic Production Time	Mosaic Description
30 m flight height %80 Overlap	1839 min	Af
60 m flight height %80 Overlap	3350 min	Bf

4. CONCLUSION

In this study, two different types of UAV were used. The production time and production accuracy of the mosaics produced with varying structures of the slope were investigated. It was considered that the results from SURF, FAST and BRISK algorithms are not adequate. An alternative application was made to compare performances and mosaics were produced from UAV images. The created mosaics were as seen in figure 8. The effort to provide these mosaics was as in table 3.

As a general function of the software that detects feature factors, they are attempting to identify distinct places that can be matched over the image. Since there are no factors inside the terrain that can produce lots of detail, the algorithms try and map the locations which can be very similar to each other as feature factors. Therefore, there was a problem in mosaic production. Mosaics produced due to mismatches and very long strategies were now not found to be satisfactory. The operating ideas of an automated software program that provide models from UAV are based on similar algorithms. However, the aforementioned software has developed different operating policies to increase accuracy by reducing the processing time. Since UAVs acquire the pixels coordinately, the images are fascinated with their approximate region known. Also, the parameters of skewness and curvature are recognized by the software close to their real position. Besides, seeing that this software is produced on a photogrammetric basis, it can expect the maximum wide variety of images that can be matched. In mild of this information, feature points of images are extracted quicker and more accurately.

ACKNOWLEDGEMENT

This research paper prepared from the doctoral thesis of Hasan Bilgehan Makineci.

REFERENCES

- Aslan, M. F., Durdu, A., & Sabanci, K. (2019). Fusion of CT and MR Liver Images by SURF-Based Registration. *International Journal of Intelligent Systems and Applications in Engineering*, 7(4), 216-221.
- Bay, H., Ess, A., Tuytelaars, T., & Van Gool, L. (2008). Speeded-up robust features (SURF). *Computer vision and image understanding*, 110(3), 346-359.
- Cen, C., Li, R., & Xu, X. (2019, June). Fast robust matching algorithm based on BRISK and GMS. In *Journal of Physics: Conference Series* (Vol. 1237, No. 2, p. 022070). IOP Publishing.

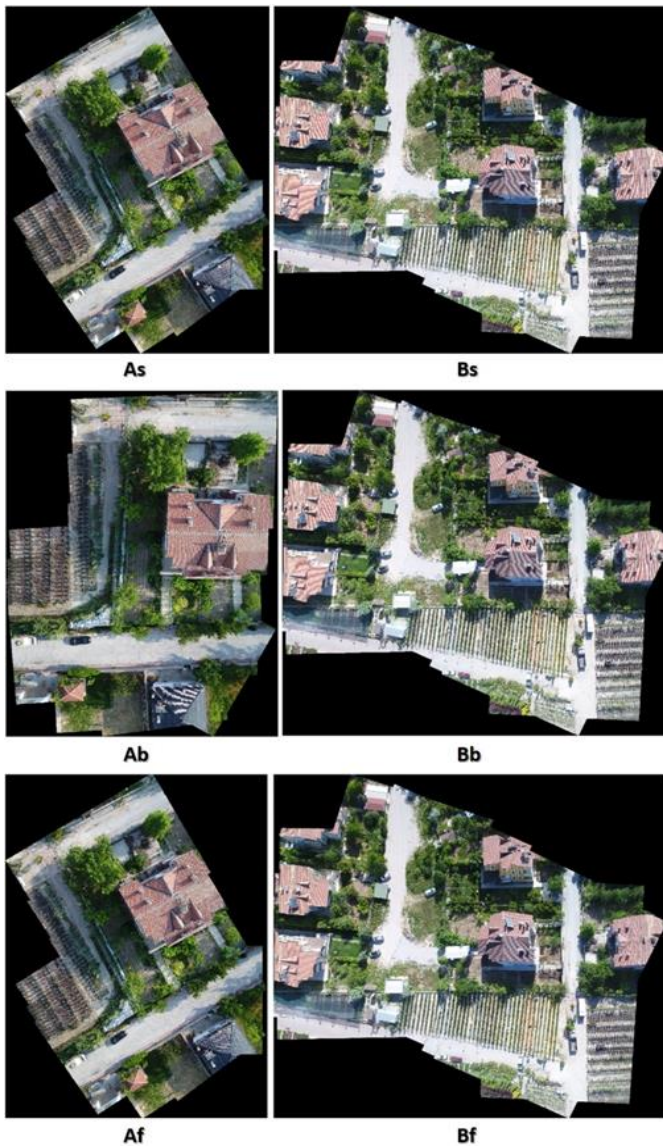


Figure 8. Mosaics of SURF, FAST and BRISK algorithms

- Durdu, A., & Korkmaz, M. (2019). Autonomously simultaneous localization and mapping based on line tracking in a factory-like environment. *Advances in Electrical and Electronic Engineering*, 17(1), 45-53. *Image, Vision and Computing (ICIVC)* (pp. 489-493). IEEE.
- Greengard, L., & Rokhlin, V. (1986). A fast algorithm for particle simulations (No. YALEU/DCS/RR-459). YALE UNIV NEW HAVEN CT DEPT OF COMPUTER SCIENCE..
- Juan, L., & Oubong, G. (2010, July). SURF applied in panorama image stitching. In *2010 2nd international conference on image processing theory, tools and applications* (pp. 495-499). IEEE.
- Leutenegger, S., Chli, M., & Siegwart, R. Y. (2011, November). BRISK: Binary robust invariant scalable keypoints. In *2011 International conference on computer vision* (pp. 2548-2555). Ieee.
- Liang, Y. J., Li, Q., Chen, D. P., & Yan, X. J. (2012). Fast and Robust LOG-FAST Corner Algorithm. *Computer Science*, 39(6), 251-254.
- Makineci, H. B. (2016). İnsansız Hava Araçları Lidar Etkileşimi. *Geomatik*, 1(1), 19-23.
- Makineci, H. B., & Karabörk, H. (2016). Evaluation digital elevation model generated by synthetic aperture radar data. *International Archives of the Photogrammetry, Remote Sensing and Spatial Information Sciences*, 1.
- Tareen, S. A. K., & Saleem, Z. (2018, March). A comparative analysis of sift, surf, kaze, akaze, orb, and brisk. In *2018 International conference on computing, mathematics and engineering technologies (iCoMET)* (pp. 1-10). IEEE.
- Rublee, E., Rabaud, V., Konolige, K., & Bradski, G. (2011, November). ORB: An efficient alternative to SIFT or SURF. In *2011 International conference on computer vision* (pp. 2564-2571). Ieee.
- Rosten, E., & Drummond, T. (2005, October). Fusing points and lines for high performance tracking. In *Tenth IEEE International Conference on Computer Vision (ICCV'05) Volume 1* (Vol. 2, pp. 1508-1515). Ieee.
- Wu, M. (2018). Research on optimization of image fast feature point matching algorithm. *EURASIP Journal on Image and Video Processing*, 2018(1), 106.
- Zhong, B., & Li, Y. (2019, July). Image Feature Point Matching Based on Improved SIFT Algorithm. In *2019 IEEE 4th International Conference on*

Determining the Effects of the 2020 Elazığ-Sivrice/Turkey (Mw 6.7) Earthquake from the Surrounding CORS-TR GNSS Stations

Sefa Yalvaç*¹ 

¹Gümüşhane University, Department of Geomatics Engineering, Gümüşhane, Turkey

Keywords

CORS-TR
Crustal Deformation
Elazığ-Sivrice Earthquake
GNSS

ABSTRACT

In this study, co-seismic displacements originating from Elazığ-Sivrice earthquake in the Eastern Anatolian Fault Zone (EAFZ) on 24 January 2020 were investigated. For this purpose, data of 11 CORS-TR stations in the nearby earthquake focal point were used. Receiver Independence Exchange (RINEX) observation data of 11 stations between the dates of 1-30 January 2020 (30 days) were obtained from CORS-TR servers and analyzed. Analyzes were carried out with GAMIT/GLOBK V10.71 software and coordinate time series were created from daily solutions. Co-seismic displacement caused by earthquake was revealed by coordinate time series and total displacements (co-seismic) were calculated by coordinate differences between the before and after the earthquake. According to the results, an earthquake-induced motion of 20-60 mm was detected at the GNSS stations located in the nearby of earthquake epicenter. In addition, vertical movement was not detected at any of the 11 CORS-TR GNSS station.

1. INTRODUCTION AND TECTONIC SETTING

Global Navigation Satellite System (GNSS) technique is widely used for geodetic and geodynamic modeling studies such as monitoring tectonic plate movements, earthquake observation, crustal deformation, etc. as it can produce high precision, low-cost and 3D positioning in a global coordinate system. An important part of these studies has been done in Anatolia due to tectonic diversity (McClusky et al., 2000; Ustun et al., 2010; Tiryakioğlu et al., 2019).

Turkey has been a natural laboratory for multidisciplinary studies involving earthquake observation and related research. Most of the studies consist of monitoring with GNSS on the North Anatolian Fault Zone (NAFZ) and Eastern Anatolian Fault Zone (EAFZ) (e.g. Ambraseys, 1989; Ozener et al., 2010; Tiryakioğlu et al., 2017; Tiryakioğlu et al., 2018; Bletery et al., 2020), which

produces large and destructive earthquakes (Figure 1).

The EAFZ starts from Karlıova in the northeast and extends to Kahramanmaraş in the southwest and forms the southeast border of the Anatolian plate. It is about 500 km long between the Arabian and Anatolian plates and is a left-lateral strike-slip fault zone. The left lateral movement along the fault zone contributes to the escape of Anatolia to the west (Allen 1969; Dewey et al., 1986). Relative plate motion occurs with slip rates ranging from 6 to 10 mm/year and has resulted in destructive earthquakes in eastern Turkey (Bulut et al., 2012).

Considering the historical earthquake activity of EAFZ in past 60 years, some of the most important earthquakes on this fault are 1964 Malatya *Ms* 5.7, 1971 Bingöl *Ms* 6.9, 1977 Palu *Mw* 5.2, 1986 Doğanşehir-Malatya *Ms* 5.9, 2003 Bingöl *Mw* 6.3, 2004 Sivrice *Mw* 5.5 and 2010 Kovancılar-Elazığ *Mw* 6.1.

* Corresponding Author

(sefayalvac@gumushane.edu.tr) ORCID ID 0000-0002-8989-6231

Cite this article

Yalvac, S. (2020). Determining the Effects of the 2020 Elazığ-Sivrice/Turkey (Mw 6.7) Earthquake from the Surrounding CORS-TR GNSS Stations by means of Relative GNSS Analysis. Turkish Journal of Geosciences, 1(1), 15-20.

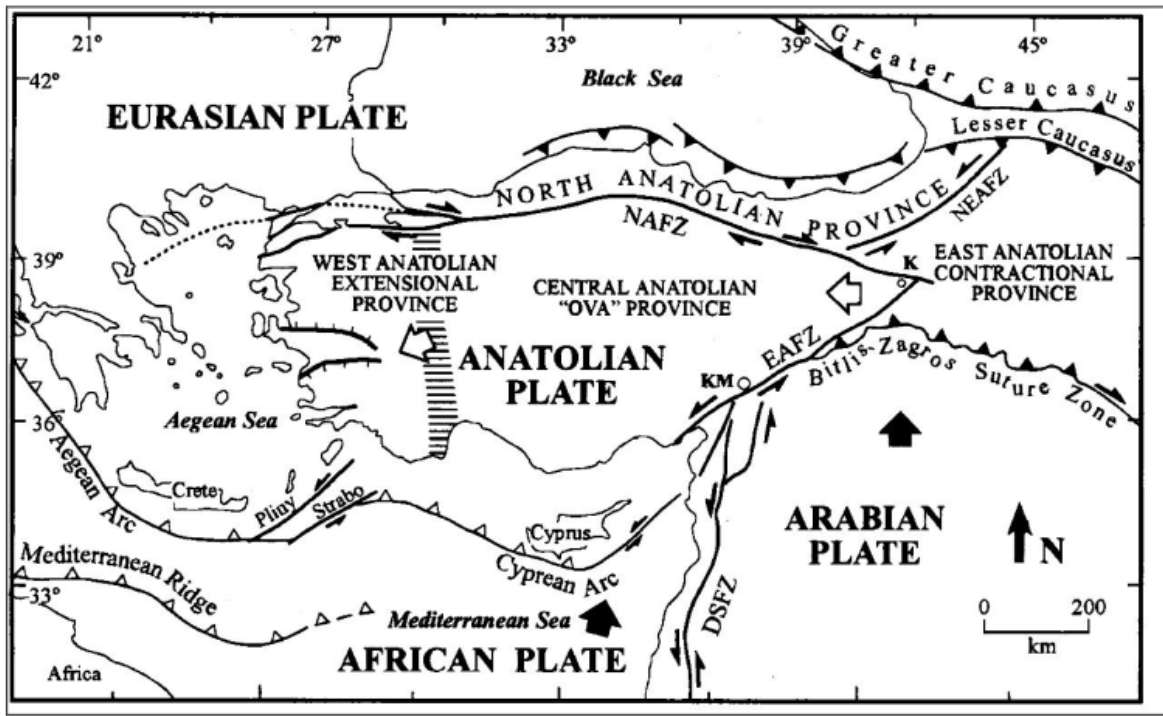


Figure 1. Important neotectonic structures in Turkey (Bozkurt, 2001).

The latest earthquake recorded on EAFZ was the Doğanyol-Sivrice earthquake (Fig. 2) with Moment magnitude (M_w) 6.7 on January 24, 2020 (Lat: 38.3590 N, Long: 39.0628 E). The depth of the earthquake, which is strongly felt in Malatya and Diyarbakır, especially in Elazığ, is reported as 8 km

(AFAD, 2020). According to AFAD (2020), it is assumed that the approximately 55-60 kilometers-long fault segment of the EAFZ zone, located in the southwest of the Hazar Lake, west of Sivrice and Pötürge district, has been broken up bilaterally and caused the Elazığ-Sivrice earthquake (Fig. 2).

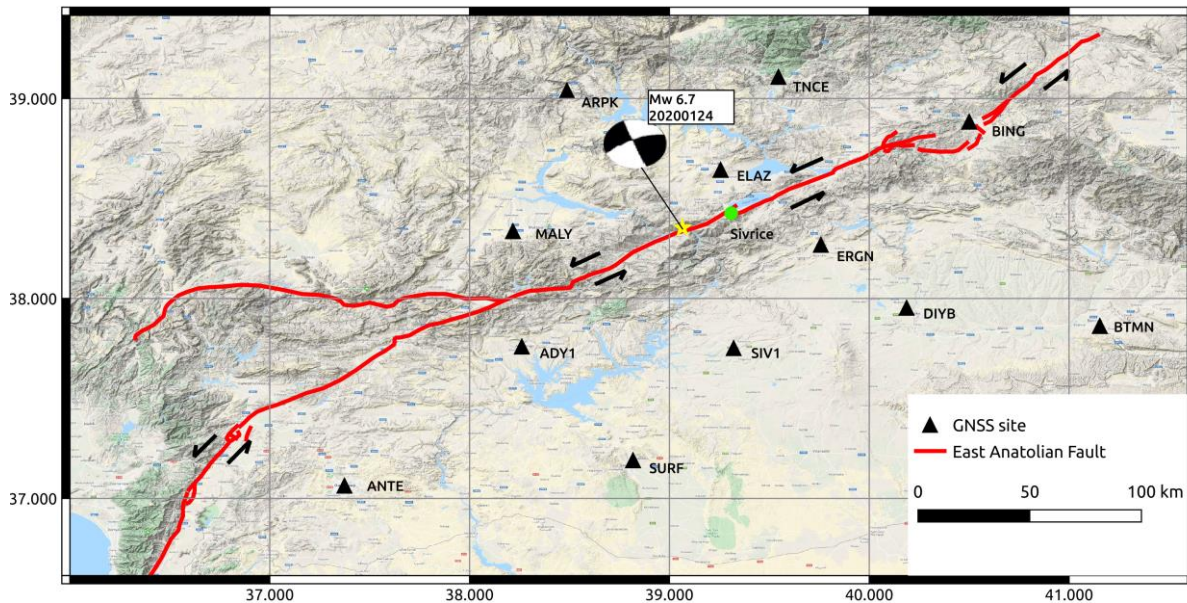


Figure 2. The East Anatolian Fault Zone (EAFZ), epicenter of the Doğanyol-Sivrice Mw 6.7 earthquake (yellow star) and surrounding CORS-TR GNSS stations

2. GEODETIC STUDY OF THE EARTHQUAKE

Determining the amount of displacement generated by earthquakes will play an important role in revealing the earthquake kinematics and consequently understanding the related tectonic movements. In this context, the data of Continuously Operating Reference Station (CORS) GNSS stations nearby of the earthquake epicenter provides great convenience. The CORS stations located in Turkey called as CORS-TR network consists of 146 GNSS reference stations and was mainly designed to provide Real-Time Kinematic (RTK) applications. However, reference station data of this network with 30 seconds interval is archived and provides important contributions to reveal crustal deformations.

In this study, 11 GNSS stations data of CORS-TR network located nearby of the epicenter of the Elazig-Sivrice earthquake are obtained and analyzed. The analyzes cover the period from the day of the year (DoY) of 1 to the 30th of 2020 and were carried out with the GAMIT/GLOBK V10.71 software according to the relative GNSS analysis technique (Herring et al., 2010). The earthquake-related displacements were estimated by examining the time series produced from daily solutions.

3. GNSS NETWORK DESIGN AND ANALYSIS

As mentioned in the previous section, eleven stations (ANTE, MALY, ADY1, SURF, SIV1, ARPK, TNCE, ELAZ, ERGN, DIYB, BING, and BTMN) from CORS-TR network were used in this study (Fig. 2). In order to make earthquake effect clearly (co-seismic displacement) visible in the time series, thirty-day consecutive data were analyzed from January 1 to January 30 of 2020. The (Receiver Independence Exchange) 24 hours of RINEX observation files with 30 seconds interval were obtained from CORS-TR servers for 30 days period.

Daily 24-hour of RINEX observation files from the 11 stations were processed using GAMIT/GLOBK V10.71 software. The analyses were carried out in two basic steps. In the first step, the relative coordinates were estimated on the basis of the weighted least squares algorithm using the ionosphere-free linear combination (LC) of the phase observable by the GAMIT module. The orbital and clock parameters were obtained from International GNSS Service (IGS) and minimum constraint (with respect to the ANKR site) procedure was used for ambiguity fixing in 5 cm for both horizontal and vertical directions. In the second step, the reference frame definition was performed for the daily solutions by using the GLRED module. Then, a 7-parameter Helmert transformation was applied and its parameters were estimated by means of 10 IGS stations (ANKR, ARUC, BSHM, HAMD, ISTA, MATE, NICO, ORID,

TUBI, and ZECK) with coordinates and the velocity defined in ITRF14.

4. GNSS-DERIVED DISPLACEMENT

From the daily solutions, time series were created by combining the coordinates estimated with a precision of 2-3 mm in the horizontal direction and 7-8 mm in the vertical direction during the monitoring period (30-days). Time series belonging to ELAZ and ERGN stations, where significant movement is obtained since it is closest to the earthquake epicenter, is presented in Figures 3 and 4 for the horizontal direction.

By comparing to the station coordinates of the CORS-TR GNSS sites from daily solutions before and after the Elazig-Sivrice earthquake (DoY 24), obtained the co-seismic displacement.

The co-seismic displacements from monitoring period results were determined according to Equation (1).

$$\begin{aligned}\Delta n_{\text{cos}} &= n_{\text{post}} - n_{\text{pre}} \\ \Delta e_{\text{cos}} &= e_{\text{post}} - e_{\text{pre}} \\ \Delta u_{\text{cos}} &= u_{\text{post}} - u_{\text{pre}}\end{aligned}\quad (1)$$

Where Δn_{cos} , Δe_{cos} and Δu_{cos} are the co-seismic displacements, n_{post} , e_{post} , u_{post} , n_{pre} , e_{pre} and u_{pre} indicate the average GNSS based positions estimated from before (23 days) and after (6days) the earthquake. Co-seismic displacement values obtained for 11 CORS-TR GNSS stations according to the above procedure are presented in Table 1.

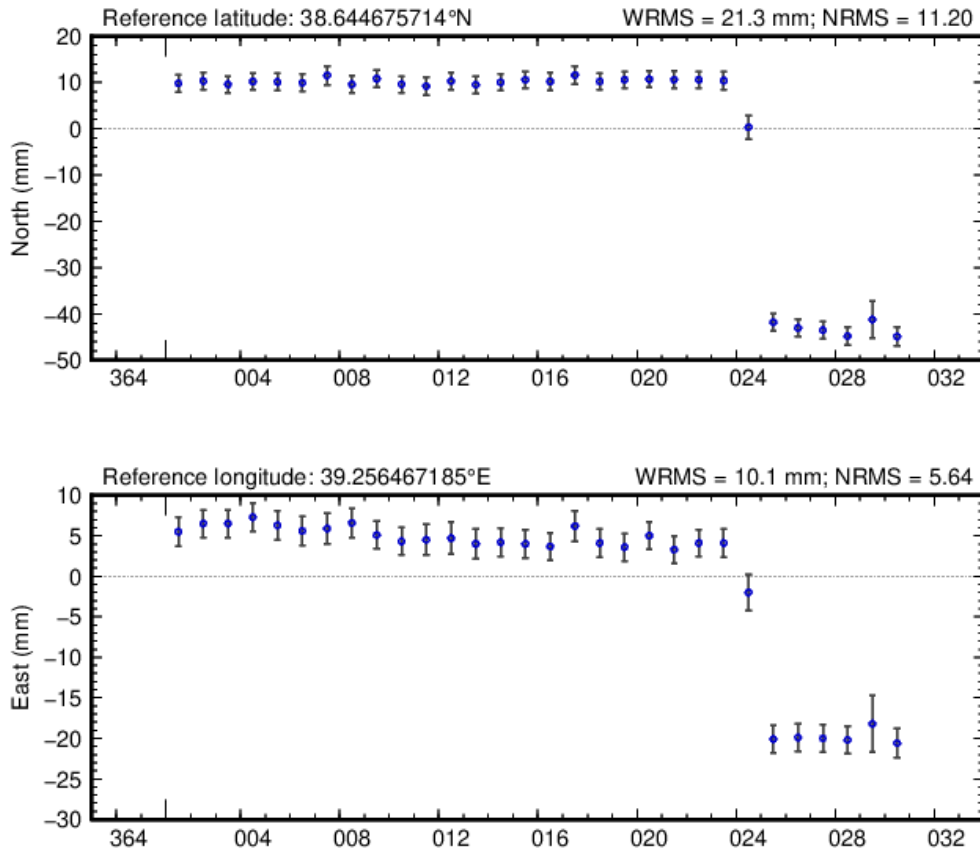


Figure 3. Coordinate time series obtained for ELAZ station during monitoring

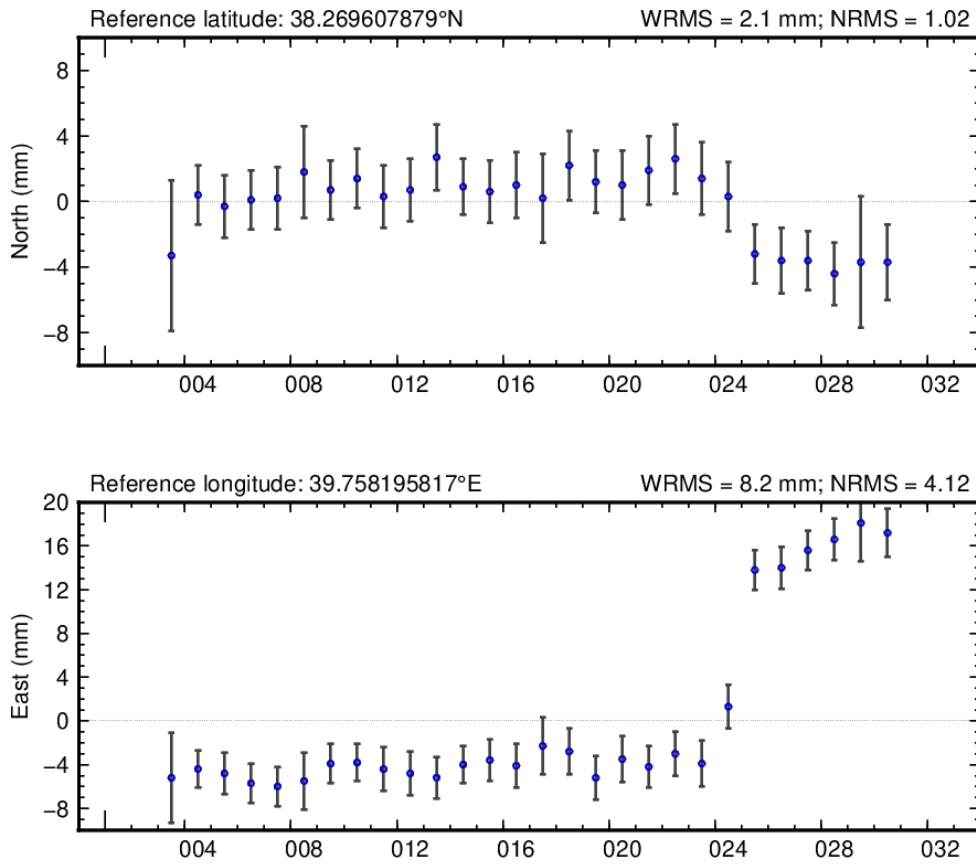


Fig 4. Coordinate time series obtained for ERGN station during monitoring

Table 1. Co-seismic displacement values calculated with Equation 1 for the CORS-TR stations (in mm).

Station	North	East	Up
BTMN	1.0	3.0	-2.9
BING	-0.4	1.2	1.0
DIYB	-0.4	6.6	3.2
ERGN	-6.5	20.2	-3.6
TNCE	-8.1	-2.4	-1.1
SIV1	3.1	5.6	-0.9
ELAZ	-53.5	-20.9	0.5
SURF	4.0	2.4	0.9
ADY1	5.7	2.8	-0.1
MALY	4.5	-16.6	-2.5
ANTE	5.7	2.8	-0.3

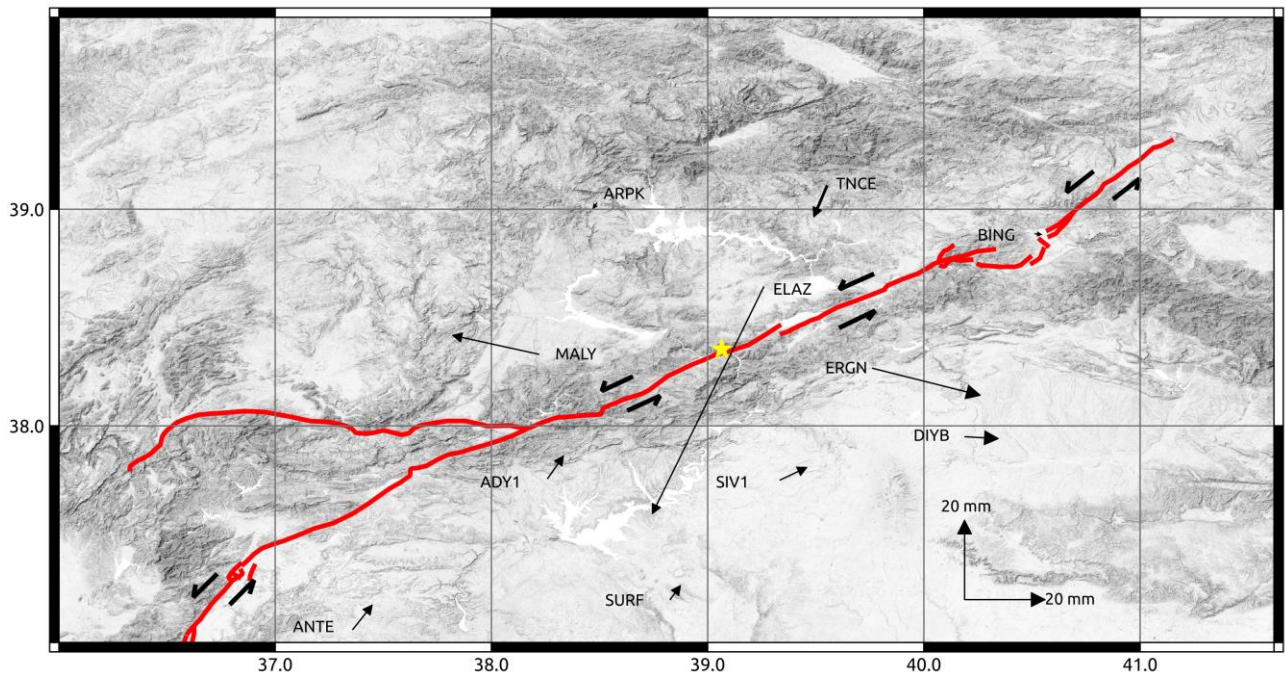


Figure 5. Earthquake-induced horizontal displacement vectors

5. DISCUSSION AND CONCLUSION

In this study, horizontal and vertical displacements (co-seismic) caused by 24 January 2020 Elazığ-Sivrice/Turkey (Mw 6.7) Earthquake have been successfully estimated by means of the relative GNSS analysis technique. For this purpose, 11 GNSS stations which belong to CORS-TR data nearby earthquake epicenter are used. Horizontal direction displacements, estimated from the 30-day coordinate time series, were successfully estimated with precision sub-mm, and vertical motions with the precision of 2-3 mm. The results obtained from displacement estimation are listed below:

- The highest horizontal displacement value with 57 mm magnitude in the South-West direction was obtained at the ELAZ station located in the north of EAFZ and approximately 30 km from the earthquake epicenter.
- In the ERGN and MALY stations, which are approximately 70 km from the earthquake epicenter and located on opposite sides of the EAFZ, 21 mm and 17 mm opposite directional horizontal motion were detected, respectively.
- The horizontal motion obtained at other stations is less than the three stations mentioned above, and the horizontal motion estimated at the stations is related to the distance from the earthquake epicenter.
- No vertical movement due to the earthquake was obtained at any station.

REFERENCES

- Allen, C. R. (1969). Active faulting in northern Turkey. Rep. 1577, 32 pp., Div. of Geol. Sic., Calif. Inst. of Technol., Pasadena.
- Ambraseys, N. N. (1989). Temporary seismic quiescence: SE Turkey. *Geophysical Journal International*, 96(2), 311-331.
- Bletery, Q., Cavalié, O., Nocquet, J. M., & Ragon, T. (2020). Distribution of interseismic coupling along the North and East Anatolian Faults inferred from InSAR and GPS data. arXiv preprint arXiv:2003.02001.
- Bozkurt, E. (2001). Neotectonics of Turkey—a synthesis. *Geodinamica acta*, 14(1-3), 3-30.

- Bulut, F., Bo M., Eken, T., Janssen, C., Kılıç, T., & Dresen, G. (2012). The East Anatolian Fault Zone: Seismotectonic setting and spatiotemporal characteristics of seismicity based on precise earthquake locations. *Journal of Geophysical Research: Solid Earth*, 117(B7).
- Dewey, J. F., Hempton, M. R., Kidd, W. S. F., Saroglu, F. A. M. C., & Şengör, A. M. C. (1986). Shortening of continental lithosphere: the neotectonics of Eastern Anatolia—a young collision zone. *Geological Society, London, Special Publications*, 19(1), 1-36.
- Dong, D., Herring, T. A., & King, R. W. (1998). Estimating regional deformation from a combination of space and terrestrial geodetic data. *Journal of Geodesy*, 72(4), 200-214.
- Gokceoglu, C., Şahmaran, M., Unutmaz, B., Aldemir, A., Kockar, M., Sandikkaya, A., İçen, A. (2020). Hacettepe Üniversitesi Mühendislik Fakültesi İnşaat Mühendisliği Bölümü 24 OCAK 2020 - Elazığ Sivrice Depremi Ön İnceleme Raporu, 10.13140/RG.2.2.30561.45921.
- Herring, T. A., King, R. W., & McClusky, S. C. (2010). Introduction to Gamit/Globk. Massachusetts Institute of Technology, Cambridge, Massachusetts.
- McClusky, S., Balassanian, S., Barka, A., Demir, C., Ergintav, S., Georgiev, I., ... & Kastens, K. (2000). Global Positioning System constraints on plate kinematics and dynamics in the eastern Mediterranean and Caucasus. *Journal of Geophysical Research: Solid Earth*, 105(B3), 5695-5719.
- Ozener, H., Arpat, E., Ergintav, S., Dogru, A., Cakmak, R., Turgut, B., & Dogan, U. (2010). Kinematics of the eastern part of the North Anatolian Fault Zone. *Journal of geodynamics*, 49(3-4), 141-150.
- Tiryakioğlu, I., Yigit, C. O., Ozkaymak, C., Baybura, T., Yilmaz, M., Ugur, M. A., ... & Gulal, V. E. (2019). Active surface deformations detected by precise levelling surveys in the Afyon-Akşehir Graben, Western Anatolia, Turkey. *Geofizika*, 36(1), 33-52.
- Tiryakioğlu, I., Yavasoglu, H., Ugur, M. A., Özkaymak, C., Yilmaz, M., Kocaoglu, H., & Turgut, B. (2017). Analysis of October 23 (Mw 7.2) and November 9 (Mw 5.6), 2011 Van Earthquakes Using Long-Term GNSS Time Series. *Earth Sciences Research Journal*, 21(3), 147-156.

Tiryakiođlu, İ., Aktuđ, B., Yiđit, C. Ö., Yavařođlu, H. H., Sözbilir, H., Özkaymak, Ç., ... & Özener, H. (2018). Slip distribution and source parameters of the 20 July 2017 Bodrum-Kos earthquake (Mw6. 6) from GPS observations. *Geodinamica Acta*, 30(1), 1-14.

Ustun, A., Tusat, E., & Yalvac, S. (2010). Preliminary results of land subsidence monitoring project in Konya Closed Basin between 2006-2009 by means of GNSS observations. *Natural Hazards and Earth System Sciences*, 10(6), 1151.

AFAD, (2020, April 20). 24 January 2020 Sivrice-Elazig Mw 6.8 Earthquake Preliminary assessment report Retrieved from <https://deprem.afad.gov.tr/downloadDocument?id=1825>

Determining The Forest Fire Risk with Sentinel 2 Images

Rutkay Atun ¹, Kaan Kalkan ^{*2}, Önder Gürsoy ¹

¹Sivas Cumhuriyet University, Faculty of Engineering, Department of Geomatics Engineering, Sivas, Turkey

²Tübitak Uzay, Head of Remote Sensing Group, Ankara, Turkey

Keywords

Forest fire
Fire severity indices
Fire risk
Sentinel 2

ABSTRACT

Forest fires are one of the most important disasters since past. The necessary preventions should be taken promptly to prevent these disasters. Remote sensing, which is a very effective and practical tool, is one of these tools that provide a timely receipt of measures with the development of technology. In this study, a forest fire that started at 07.23.2018 in Athens, in Greece and continued until July 26 was discussed. Mati region where the most loss of life was examined as the study area. Sentinel 2 images were used in order to detect forest fire risk class. Normalized Burn Ratio (NBR), Differenced Normalized Burn Ratio (dNBR), Relativized Burn Ratio (RBR) spectral indices and Normalized Difference Vegetation Index (NDVI) were used in order to determine the forest area damaged by fire and to establish fire risk classes. According to the results of the study, the size of the vegetation area that was destroyed due to fire determined, and the probability of forest fire exposure of these areas established.

1. INTRODUCTION

Forest fires are one of the most important disasters of our time. An increasing trend in forest fires has been observed all over the world from past to present. There are 2 main factors that cause forest fires: Nature and human. Unplanned urbanization, sabotage, carelessness, recklessness, and global warming are among the few factors that cause forest fires. In recent years, many big forest fires have occurred in the world. 271,350 ha in Greece in 2007, 450,000 ha in 2009 in Australia, 500,000 ha in Russia in 2010, and 25,000 ha in Bolivia in 2010 were destroyed due to fires. A total of 1,200,000 ha of land was destroyed by the forest fire in Canada in 1825, and this was recorded as the largest known forest fire in history. (Özkazanç and Ertuğrul, 2011; Francos et al., 2016). These fires, which cause damage to large natural areas, lead to disruption of the natural ecosystem, cause human and living creature deaths.

While preventing forest fires requires a very important environmental management, identifying forest fire risk areas is another pillar of environmental management. With the identification

of risk areas, necessary precautions will be taken on time, the number of forest fires will be reduced or minimized. Remote sensing could be used to identify areas damaged by forest fires, and besides, these areas could be classified according to forest fire possibility. Remote sensing also provides speed, practicality, and efficiency in detecting and monitoring forest fire risk areas. Nowadays, with the development of technology, the use of remote sensing in the detection of forest fires, damage detection studies and the detection of risky areas has increased gradually and there are many studies on this subject (Kerr and Ostrovsky, 2003; Boer et al., 2008; Delgado et al., 2010; Matin et al., 2017; Navarro et al., 2017; Yuan et al., 2017).

Different methods can be applied in these studies related to a forest fire in remote sensing. Fire-damaged areas could be identified by classifying optical satellite images such as Landsat or MODIS. Object-based classification and spectral classification are some of these methods. In addition, calculating land surface temperature with thermal bands of optical images is used to determine fire areas. Besides, topographic parameters such as elevation, slope, and aspect could be produced from

* Corresponding Author

(ratun@cumhuriyet.edu.tr) ORCID ID 0000-0001-9959-2058
(kaankalkan@gmail.com) ORCID ID 0000-0002-2732-5425
(ogursoy@cumhuriyet.edu.tr) ORCID ID 0000-0002-1531-135X

Cite this article

Altun, R., Kalkan, K., Gürsoy, Ö. (2020). Determining The Forest Fire Risk with Sentinel 2 Images. Turkish Journal of Geosciences, 1(1), 21-25.

Received: xx/xx/xxxx; Accepted: xx/xx/xxxx

the Shuttle Radar Topographic Mission (SRTM) in order to determine fire risk severity. Topographic factors can be integrated into a geographic information system and these areas can be determined by giving certain weights to them. Also, spectral fire indices are used to identify forest fire zones and risk areas (Delgado et al., 2010; Comert et al., 2017; Matin et al., 2017; Navarro et al., 2017; Comert et al., 2019).

In this study, a forest fire that started on July 23 and continued until July 26 in Athens, Greece, was discussed. The fire occurred in 2018 and caused many damages. The fire started simultaneously at many different points. That's why the cause of the fire was considered arson. A total of 79 people were killed and more than 100 people were injured due to the fire. Most of the people who died were reported to be from the Mati region in the northeast. This study aims to detect the area destroyed by fire with remote sensing and also to evaluate the fire risk of other areas. In this context, Sentinel 2 satellite images and Normalized Burn Ratio (NBR), Differential Normalized Burn Ratio (dNBR), Relativized Burn Ratio (RBR) spectral fire indices were used to create fire risk classes. In addition, Normalized Difference Vegetation Index (NDVI) was utilized to identify the forest area damaged by fire.

2. MATERIALS AND METHODS

2.1. Study Area and Materials

The study area is the Mati region, one of the areas where fires occur simultaneously, in the north-east of Athens, Greece. The texture of the region consists of a mixture of forest and urban - wooded areas including summer houses and hotels (figure 1). The Mediterranean climate is dominant in the region and scrub-type pine forests are common.

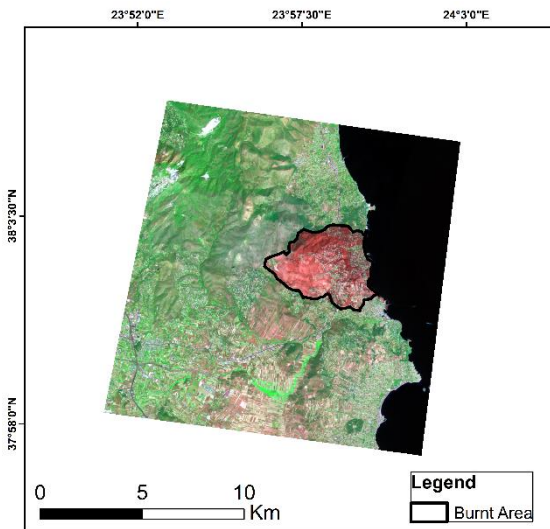


Figure 1. Study area (Red areas indicate the burnt area)

Sentinel 2 images were used as satellite images within the scope of the study. Sentinel 2 was placed in orbit by the ESA (European Space Agency) in 2015. It has also 13 bands that could obtain multispectral images (Clevers et al., 2017; (table 1)).

Table 1. The satellite images used in the study

Satellite Image	Date
S2B_MSIL1C_20180705T091019	05.07.2018
L1C_T35SKC_A007655_20180824T091603	24.08.2018
S2B_MSIL1C_20181222T091359	22.12.2018

2.2. Method

The satellite images used within the scope of the study were obtained free of charge from the United States Geological Survey (USGS) site in the UTM projection system as defined in the 34th region. In order to eliminate or minimize topographic factors, atmospheric effects, shadow effects, and sensor-induced errors on satellite images, atmospheric correction is required (Canbaz et al., 2018; Kalkan and Maktav, 2018). The atmospheric correction of the images was performed first, for this reason.

NBR, dNBR and RBR were performed as spectral indices of forest fire. The indices utilized were derived from the near-infrared and short wave infrared regions of the electromagnetic spectrum (Table 2).

Table 2. The forest fire indices used in the study

Spectral Indices	Formula Description
NBR	$NBR = (NIR - SWIR) / (NIR + SWIR)$
dNBR	$dNBR = [NBR_{pre-fire} - NBR_{post-fire}]$
RBR	$RBR = dNBR / (NBR_{pre-fire} + 1.001)$

The indices were created through images taken immediately after the fire (pre) and a few months later (post). Among the indices used in the study, the pixels in the RBR take values between -2 and +2, while in the NBR and dNBR take values between -1 and +1. In the assessment of fire risk, pixels with an index value greater than 0.55 are high; 0.25 to 0.54 moderate and 0.1 to 0.24 were categorized as low fire severity (Key and Benson, 2006). Besides, the NDVI was used to detect vegetation status and destruction before and after the fire. NDVI is also an index sensitive to the red and near-infrared regions of the electromagnetic spectrum. While the values representing vegetation cover between 0 and 1 in the index, it means that the density of the plants increases when the pixel values approach 1 (Tucker, 1979). The Indices were created using images just before the forest fire occurred and just after the fire occurred. The following pixel ranges are used to classify the pixels in the indices (Holben, 1986; (Table 3)).

Table 3. NDVI classification pixel range

Pixel Range	Class
<0	water
0.03 – 0	bare soil
0.03 – 0.3	sparse vegetation
0.3 – 0.5	moderate vegetation
0.5>	dense vegetation

3. RESULTS

Using fire indices and NDVI, areas that pose a fire risk and vegetation cover destroyed by fire have been identified. First of all, dNBR and RBR were applied to images, respectively. Then, the indices' results are classified according to pixel values and the regions that pose fire risk has been determined (figure 2).

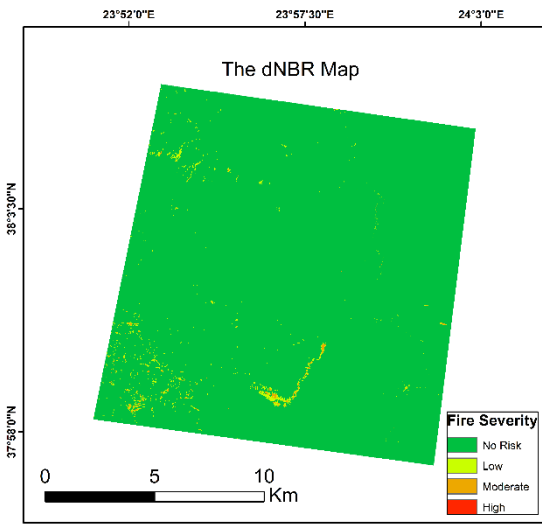


Figure 2. The dNBR map

According to the risk severity map made according to the dNBR index, it is understood that almost all of the study area does not pose a risk of a forest fire. Also, the sizes of these classes were calculated (Table 4).

Table 4. Distribution of calculated areas after applying dNBR

Fire Severity	Area (km ²)
No Risk	232.281
Low	1.9912
Moderate	0.4308
High	0.0016

After the RBR was calculated, the classification was made and the areas with risk of fire were identified (Figure 3). According to the results obtained, a large part of the field of study was in the low-risk category.

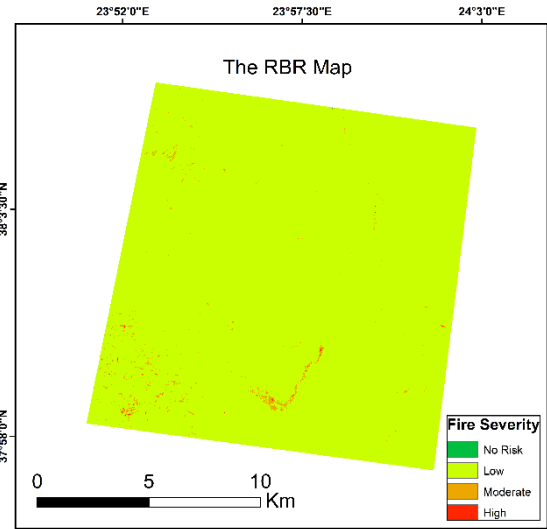


Figure 3. The RBR map

Afterward, the sizes of these areas were calculated (Table 5).

Table 5. Distribution of calculated areas after applying RBR

Fire Severity	Area (km ²)
No Risk	0.0016
Low	233.1837
Moderate	1.4421
High	0.0768

In addition, the NDVI was calculated using images taken just before and after the fire in order to determine the vegetation status before and after the fire (Figure 4-5).

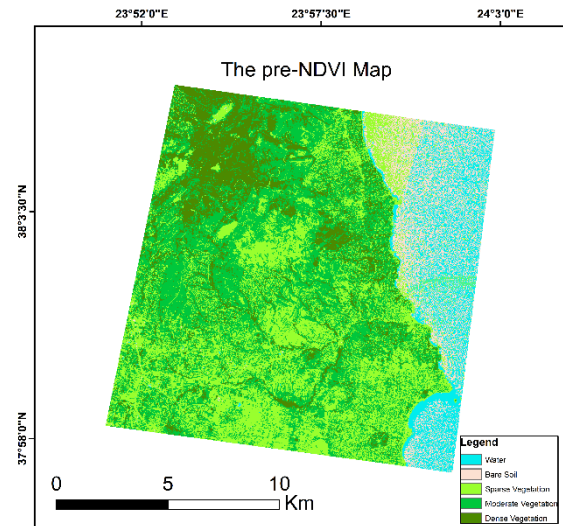


Figure 4. The pre-NDVI map (Indicates the vegetation condition before the fire)

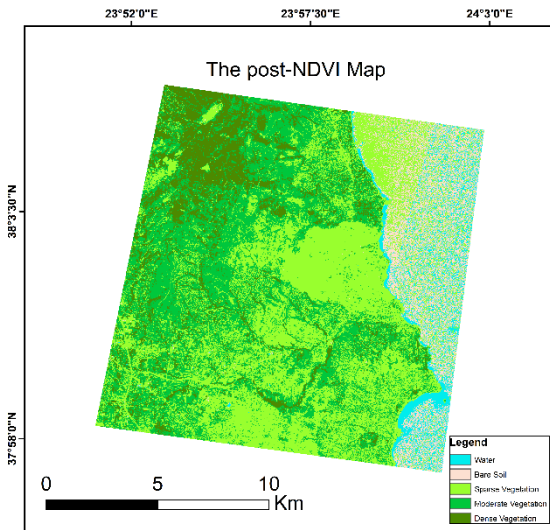


Figure 5. The post-NDVI map (Indicates the vegetation condition after the fire)

It was seen that some pixels in the water class in the NDVI map were assigned to the bare earth class. This is thought to be due to the fact that the fine fog and cloud layer above the water affects the classification accuracy. This was caused by the fact that the pixels in the bare soil were classified by taking the values between 0 and 0.03 and the cloud getting 0.02 in NDVI. To analyze the vegetation change after the fire, the NDVI status in the burnt area illustrated in the study area was also examined. It is understood that the number of dense vegetation and moderate vegetation classes decreased, while the pixels in the sparse vegetation class increased, according to NDVI (Table 6).

Table 6. Vegetation density before and after the fire

Vegetation Density	Pre Fire (m ²)	Post Fire (m ²)
Sparse Vegetation	34121	139101
Moderate Vegetation	79198	6334
Dense Vegetation	32728	413

Besides, in the NDVI map, the pixel values of the area destroyed by fire ranged between 0.1 and 0.3. Therefore, in the NDVI maps obtained after the fire, these regions are assigned as sparse vegetation and moderate vegetation as a result of classification (Figure 6).

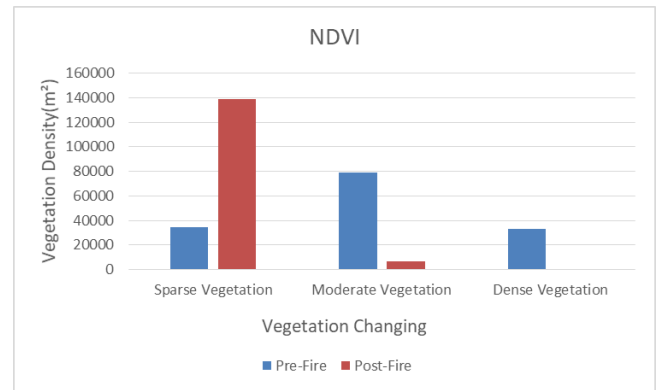


Figure 6. Vegetation distribution before and after the fire

4. DISCUSSION AND CONCLUSION

According to index results, it was understood that the RBR generates more sensitive results in determining the forest fire risk classes according to the dNBR. Also, it has been understood that the classified pixels in RBR pose more risk in terms of a forest fire risk than the same classified pixels in dNBR. dNBR is a powerful tool to detect burned area but also it is sensitive to water and thus sometimes, pixels that are classified as high severity maybe water (Bolton et al., 2015). However, since there is no water body in the study area, a water mask was not performed. According to the fire risk maps, it is seen that the areas with high forest fire risk in the study area are quite low. This is due to the fact that the study area consists of a mixture of urban texture together with the sparse forest cover. In addition, the fact that both forest and urban texture within one pixel in some pixels have affected the results by causing mixed pixel problems. On NDVI maps, these regions are classified as moderate vegetation and sparse vegetation. As supported by the results obtained from the fire index maps, it was concluded that a forest fire that may occur in this region is quite difficult to come out for natural reasons. This led to the thought that the incident in Mati in 2018 was due to arson. In addition, the fact that the fire started simultaneously at different points strengthens this argument.

In this study, by evaluating the forest fire that occurred in Athens Mati on 23.07.2018, risk classes for future fires in this region were estimated. Besides, the detection of vegetation that was destroyed by fire was also carried out. It is thought that using a higher resolution satellite image or an image obtained with a multispectral camera mounted on UAV will increase the accuracy of the study. In addition, categorizing the trees in the vegetation texture according to their types will increase the accuracy of the study. This methodology was not followed in this study since the restricted spatial resolution of the satellite images used in the study did not allow the classification of tree species

in the forest texture and the data of the stand map of the region were not available.

REFERENCES

- Barsi, J.A., Lee, K., Kvaran, G., Markham, B.L., Pedelty, J.A. (2014). The Spectral Response of the Landsat-8 Operational Land Imager. *Remote Sensing*, 6, 10232-10251.
- Boer, M.M., Macfarlane, C., Norris, J., Sadler, R.J., Wallece, J., Grierson, P.F. (2008). Mapping Burned Areas And Burn Severity Patterns In Sw Australian Eucalypt Forest Using Remotely-Sensed Changes In Leaf Area Index. *Remote Sensing of Environment*, 112, 4358-4369.
- Bolton, D.K., Coops, N.C., Wulder, M.A. (2015). Characterizing Residual Structure and Forest Recovery Following High-Severity Fire in the Western Boreal Of Canada Using Landsat Time-Series and Airborne Lidar Data. *Remote Sensing of Environment*, 163, 48-60.
- Canbaz, O., Gürsoy, Ö., Gökçe, A. (2018). Detecting Clay Minerals in Hydrothermal Alteration Areas with Integration of ASTER Image and Spectral Data in Kösedag-Zara (Sivas), Turkey. *Journal Geological Society of India*, 91(April), 483-488.
- Clevers, J.G.P.W., Kooistra, L., Van Den Brande, M.M.M. (2017). Sentinel-2 Data for Retrieving Lai and Leaf and Canopy Chlorophyll Content of a Potato Crop. *Remote Sensing*, 405(9), 1-15.
- Cömert, R., Matcı, D.K., Emir, H., Avdan, U. (2017). Nesne Tabanlı Sınıflandırma ile Yanmış Orman Alanlarının Tespiti. *Afyon Kocatepe Üniversitesi Fen ve Mühendislik Bilimleri Dergisi*, 17, 27-34.
- Cömert, R., Matcı, D.K., Avdan, U. (2019). Object Based Burned Area Mapping With Random Forest Algorithm. *International Journal of Engineering and Geosciences*, 4(2), 78-87.
- Delgado, R.D., Lloret, F., Pons, X. (2003). Influence of Fire Severity on Plant Regeneration By Means Of Remote Sensing Imagery. *International Journal of Remote Sensing*, 24(8), 1751-1763.
- Francos, M., Ubeda, X., Tort, J., Panerreda, J.M., Cerda, A. (2016). The Role of Forest Fire Severity on Vegetation Recovery after 18 Years. Implications for Forest Management of *Quercus suber* L. In Iberian Peninsula. *Global and Planetary Change*, 145, 11-16.
- Holben, B.N. (1986). Characteristics of Maximum-Value Composite Images from Temporal AVHRR Data. *International Journal of Remote Sensing*, 7(11), 1417-1434.
- Kalkan, K., Maktav, D. (2018). A Cloud Removal Algorithm to Generate Cloud and Cloud Shadow Free Images Using Information Cloning. *Journal of the Indian Society of Remote Sensing*, 46(8), 1255-1264.
- Key, C.H., Benson, N.C. (2006). Landscape assessment: ground measure of severity, the composite burn index; and remote sensing of severity, the Normalized Burn Ratio. In: Lutes, D.C., Keane, R.E., Caratti, J.F., Key, C.H., Benson, N.C., Sutherland, S., Gangi, L.J. (Gtr.), FIREMON: Fire effects monitoring and inventory system (pp. 1-55), Washington DC.
- Kerr, J.T., Ostrosky, M. (2003). From Space To Species: Ecological Applications For Remote Sensing. *TRENDS in Ecology and Evolution*, 18(6), 299-305.
- Matin, M.A., Chitale, V.S., Murthy, M.S.R., Uddin, K., Bajracharya, B., Pradhan, S. (2017). Understanding Forest Fire Patterns And Risk In Nepal Using Remote Sensing, Geographic Information System And Historical Fire Data. *International Journal of Wildland Fire*, 26, 276-286.
- Navarro, G., Caballero, I., Silva, G., Parra, P.C., Vazquez, A., Calderia, R. (2017). Evaluation of forest fire on Madeira Island using Sentinel-2A MSI imagery. *International Journal of Applied Earth Observation and Geoinformation*, 58, 97-106.
- Tucker, C.J. (2017). Red and photographic infrared linear combinations for monitoring vegetation. *Remote Sensing of Environment*, 8(2), 127-150.
- Yuan, C., Liu, Z., Zhang, Y. (2017). Aerial Images-Based Forest Fire Detection for Firefighting Using Optical Remote Sensing Techniques and Unmanned Aerial Vehicles. *The Journal of Intelligent and Robotic Systems*, 88, 635-654.

Comparison of different classification algorithms for the detection of changes on water bodies; Karakaya Dam Lake

Ahmet Tarık Torun*¹, Halil İbrahim Gündüz¹

¹Aksaray University, Faculty of Engineering, Department of Geomatics Engineering, Aksaray, Turkey

Keywords

Classification
Change detection
Water bodies

ABSTRACT

Optimum management of water and water bodies is crucial in ensuring and maintaining the natural ecosystem cycle. Benefits from wetlands in the world and in our country keep humanity alive. Resources that are of vital importance should be monitored and changes should be observed. Thanks to the science of remote sensing, researchers in many parts of the world can monitor changes in the waters of the earth through satellite imagery and terrestrial supporting studies. The main component of change detection in remote sensing is the classification process. Nowadays, the Classification process has reached different dimensions with the contributions of artificial intelligence and machine learning algorithms. The emergence of different classification algorithms also affected the results obtained from the analyzes. In this study, the change occurred between 1990-2000-2010-2019 in Karakaya Dam Lake, which is included in the borders of Malatya - Elazığ provinces, was observed. In this context, supervised classification processes and change detection analyzes were performed using Landsat satellite data with maximum likelihood, artificial neural network, support vector machine and decision tree algorithms. For detecting the change analysis, the lake boundaries obtained from official sources were used and compared. The data obtained as a result of the study were compared for each algorithm and the amount of change was interpreted.

1. INTRODUCTION

Water is an important component in ensuring the life cycle on Earth. It is important to monitor the wetlands around the world and protect them in order to obtain optimum benefit from them (Lu et al., 2011). At the same time, water is an indispensable strategic element for human survival and social development (Ridd and Liu, 1998). Wetlands are actively used in our country and over the world both for energy production and for the maintenance of natural activities. Studies such as evaluating the status of existing water resources and examining their future status, mapping, monitoring their changes, and taking wetland inventory are critical in many disciplines (Rokni et al., 2014).

In particular, changes related to water emerging in terms of global climate change raise concerns in many countries of the world (Calò et al., 2018). Temporal climate changes and drought are seen as

the main reason for the change and decrease of wetlands (Orhan et al., 2017). Remote sensing methods, which are engaged at this stage, have a large share in monitoring climate changes and changes in water areas.

Satellites with different spectral and spatial resolution used in remote sensing provide a high amount of data for detecting wetlands. The determination of wetlands with remote sensing methods has been studied for more than two decades (Sun et al., 2012; Kaplan et al., 2019). Since the launch of the Landsat-1 satellite in 1972, efforts have been made to identify the water on the image (Work and Gilmer, 1976).

The process of collecting objects with similar spectral reflectance values on the ground under the same group is called classification in remote sensing (Torun, 2015). Classification process can be done by many mathematical and statistical methods. Thanks to the renewed and developing technology, artificial

* Corresponding Author

* (ahmettarik.torun@aksaray.edu.tr) ORCID ID 0000-0002-7927-4703
(halilibrahimgunduz@aksaray.edu.tr) ORCID ID 0000-0002-0609-8032

Cite this article

Torun, A. T., Gündüz, H. İ. (2020). Comparison of different classification algorithms for the detection of changes on water bodies; Karakaya Dam Lake. *Turkish Journal of Geosciences*, 1(1), 26-33.

intelligence and machine learning algorithms are also included in these techniques. Scientists have studied and compared the accuracy of these methods in many studies (Lu and Weng, 2007; Colkesen, 2009; Fuping et al., 2011). As a matter of fact, that the more accurate you classify, the better quality analysis you will get.

In this study, it is aimed to observe the change in the coastal boundaries of Karakaya Dam lake, which is the feed factor of Karakaya dam, by using different classification algorithms. For this reason, satellite images of 1990-2000-2010 and 2019 years were provided. Training and test areas were determined to be used in classifications over the image and classifications were made using Maximum Likelihood, Artificial Neural Network, Support Vector Machine and Decision Tree algorithms. The coastline of lake produced as a result of the classifications has been compared with the limit obtained from official sources. In addition, as a result of the classifications, the 30-year change in the lake area has been revealed on areal basis.

2. METHODS

2.1. Maximum Likelihood

The Maximum Likelihood method, one of the most used image classification methods in remote sensing, is also extensively in the detection of changes in wetlands (Munyati 2000; Frazier and Page 2000; Zhang et al., 2009). In this method, the variance and covariance values are evaluated quantitatively in the classification of each unknown pixel. With the help of probability functions calculated for each pixel, it is determined which class a pixel is closer to (Mather, 1987; Kavzoglu and Colkesen, 2010). After this process is completed, the candidate pixel is assigned to the class with the highest probability value. If this value is below the threshold value determined by the user, the pixel is considered as indefinite (Lilesand et al., 2008).

Since the ML method calculates the probability of each pixel belonging to any class, it performs a lot of mathematical operations and therefore runs slightly slower than other methods. Also, since this method does not use textural and structural information in the image but only uses spectral information, it is more limited than object-based methods (Zhou and Robson, 2001; Dean and Smith, 2003; Pizzolato and Haertel, 2003).

2.2. Support Vector Machines

Support Vector Machines (SVM) is a classification algorithm widely used for the classification of remotely sensed images and high classification accuracy of the SVM has been revealed in many studies (Huang et al., 2002; Foody and Mathur, 2004; Kavzoglu and Colkesen, 2009; Mountrakis et al., 2011; Dixon and Candade, 2008). SVM is the first non-parametric, supervised

classification method based on statistical learning theory, proposed by Vapnik. The main purpose of this method to separate two classes optimally based on the determination of the decision function (hyperplane) (Vapnik, 1995).

In cases where it is not possible to define hyperplanes with linear equations, kernel functions are used. With the help of the kernel functions, data that cannot be separated linearly in the input space is displayed in a higher dimensional space and in this high dimensional space, the data is linearly separated. It is thought that the polynomial and radial-based kernels are widely used in remote sensing studies and the better results obtained with the use of radial-based kernels (Melgani and Bruzzone, 2004; Foody and Mathur, 2004; Pal and Mather, 2005; Mathur and Foody, 2008b, Kavzoglu and Colkesen, 2009).

2.3. Artificial Neural Networks

Artificial Neural Networks (ANN) can be defined as a branch of artificial intelligence developed to imitate the human brain (Viotti et al., 2002; Sahin 2012). ANN has many uses such as remote sensing modeling, stereo mapping and image compression (Goung, Zheng 1992; Lee et al., 1994; Pierce et al., 1994; Walker et al., 1994; Foody and Arora 1997). A typical ANN consists of an input layer, an output layer, and usually one or two hidden layers (Jensen et al., 1999). The purpose of ANN is to calculate the output values from the input values (Nasr et al., 2012). The neurons in the input layer take the information from outside and transfer it to the hidden layers. The information from the input layer is processed in the hidden layer and transferred to the output layer. Neurons in the output layer, on the other hand, process the information from the intermediate layer and obtain the output that must be produced for the input set presented from the input layer of the network (Oztemel, 2016). The system learns by estimating the output data from a series of input training data so that the result of any given data set can be estimated (Ingram et al., 2005). ANN, which are frequently used in Remote Sensing, are also used extensively in matters related to wetlands (Augusteijn and Warrender, 1998; Ghedira et al., 2000; Berberoglu et al., 2004).

2.4. Decision Tree

A decision tree, having its origin in machine learning theory, is a classification and pattern definition algorithm. Unlike other classification approaches that use a number of features (or bands) to perform the classification in a single decision step, the decision tree is based on a hierarchical decision chart or tree-like structure (Xu et al., 2005). Decision trees are frequently used in many applications due to the high classification procedures that tree structures and established rules are simple and understandable (Simard et al., 2000; Huang and

Yang, 2001; Pavuluri et al., 2002). The basic structure of a decision tree consists of a root node, a set of internal nodes and a set of terminal nodes. In this tree structure, each attribute information is represented by a node. The basic principle in creating a decision tree structure by using the attribute information of the education data can be expressed as asking a series of questions regarding the data and acting in line with the answers obtained, and getting the results as soon as possible (Kavzoglu and Colkesen, 2010). Due to the high accuracy it provides, the decision trees method, which has been used successfully in remote sensing, is also frequently used in wetlands (Wei et al., 2008; Berhane et al., 2018; Baghdadi et al., 2001).

3. STUDY AREA AND MATERIALS

Karakaya Dam Lake, which borders Malatya and Elazığ provinces, has been selected as a pilot area. The lake, the second largest dam on the Fırat River, which provides a significant part of Turkey's hydroelectric energy production, which feed the Karakaya Dam. Karakaya Dam Lake, which has an area of approximately 250 km², makes important contributions to the region in the fields of tourism, fishing and agriculture. In 2013, The Council of Ministers of Republic of Turkey declared the Karakaya Dam Lake as the Culture and Tourism Conservation Development area (T.C Resmi Gazete, 4153, 20 January 2013). Figure 1 shows the study area map.

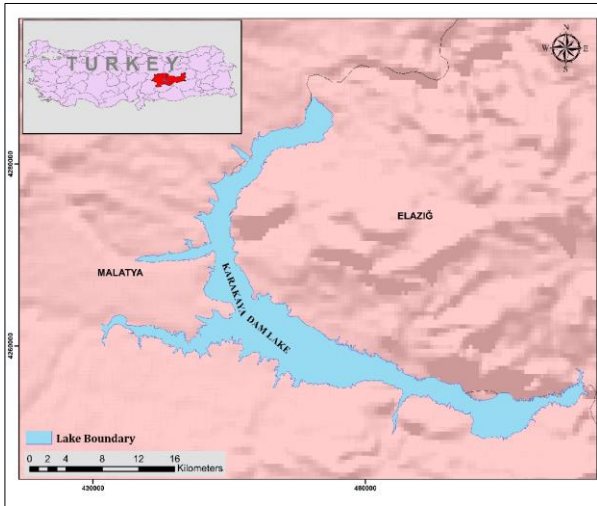


Figure 1. Study area map

Satellite images from 1990, 2000, 2010 and 2019 were obtained from the USGS data provider for use in the study. Landsat 5 TM for 1990 and 2010,

Landsat 7 ETM for 2000 and Landsat 8 OLI-TIRS satellite images were used for 2019. Red, Green, Blue and Near Infrared bands are used for all images. The data is 30 m spatial resolution and has UTM WGS-84 coordinate system and datum. Date and satellite information of the data are given in the Table 1.

Table 1. Satellite data dates and specifications

Satellite	Date	Path/Row
Landsat 5 TM	15.08.1990- 22.08.2010	173/33
Landsat 7 ETM	18.08.2000	173/33
Landsat 8 OLI-TIRS	31.08.2019	173/33

4. RESULTS

In this article, it is aimed to monitor the coastal changes in Karakaya Dam Lake by using different image classification algorithms of Machine Learning. In this context, satellite images are classified using Maximum Likelihood, Artificial Neural Network, Support Vector Machine and Decision Tree algorithms. Environment for Visualizing Images 5.3 (ENVI 5.3) and ArcGIS software were used for classification and thematic mapping. For each image, the classification process was made on the basis of water bodies, pastures, continuous urban fabric and non-irrigated arable land classes in CORINE-2018 classification system.

Images are classified using four different algorithms. Then, except for the water bodies, the other classes were combined and the class that would allow the lake boundaries to be achieved was left alone. Used machine learning algorithms have revealed different results for different years. Figure 2 show that the results of different classification algorithms for different years related to the lake area. And the overall accuracies of classifications are given Table 2.

Table 2. Classification overall accuracies

Method		Year	1990	2000	2010	2019
Maximum Likelihood			0,82	0,84	0,87	0,85
Artificial Neural Network	Neural		0,88	0,88	0,93	0,88
Support Vector Machine	Vector		0,89	0,87	0,91	0,89
Decision Trees			0,88	0,84	0,90	0,89

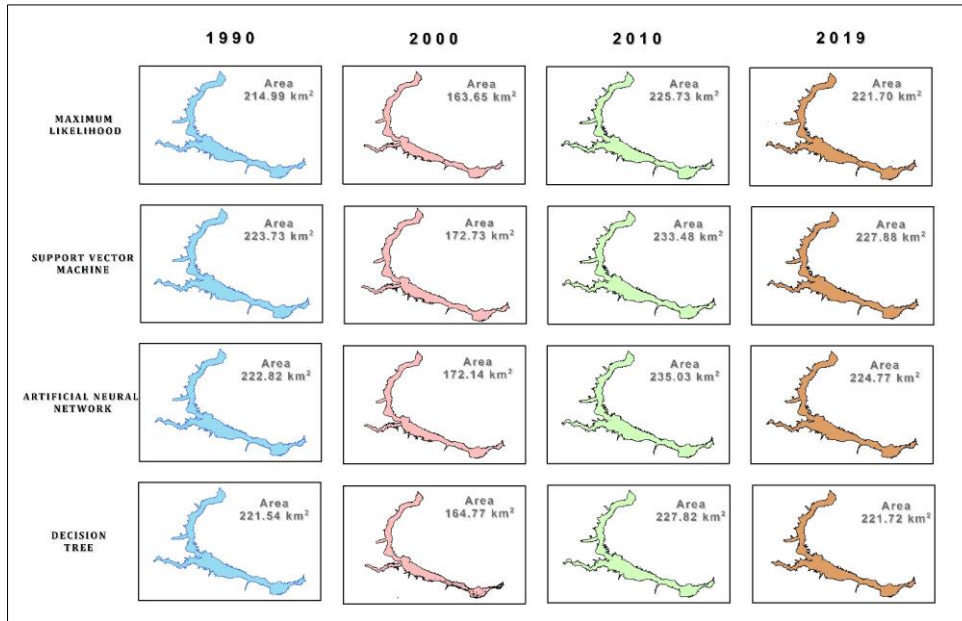


Figure 2. Classified lake coastline and area changes classified by different algorithms

With the data obtained as a result of classifications, 30-year change analyzes were applied for the lake area. As the basic data in change analysis, official coastline and lake area obtained from the 1/100000 scaled Environmental Plan which completed by the General Directorate of Spatial Planning on 19.02.2020 was used. Figure 3 shows the coastline obtained from the classifications and satellite data 10 years ago.

Thanks to the lake boundary obtained by the classification results, the change that occurs every ten years has been observed. Classification techniques were analyzed among themselves and also compared with the basic data and their differences from the basic data were calculated. Figure 4 shows the spatial change data of the

classification methods by years. Table 3 shows the spatial change that occurs when the data obtained as a result of classifications are compared with the basic data.

Table 3. Change detection analysis rates against master lake area respect years (%)

Method \ Year	1990	2000	2010	2019
Maximum Likelihood	-%16	-%36	-%12	-%13
Artificial Neural Network	-%13	-%33	-%8	-%12
Support Vector Machine	-%12	-%32	-%9	-%11
Decision Trees	-%13	-%36	-%11	-%13

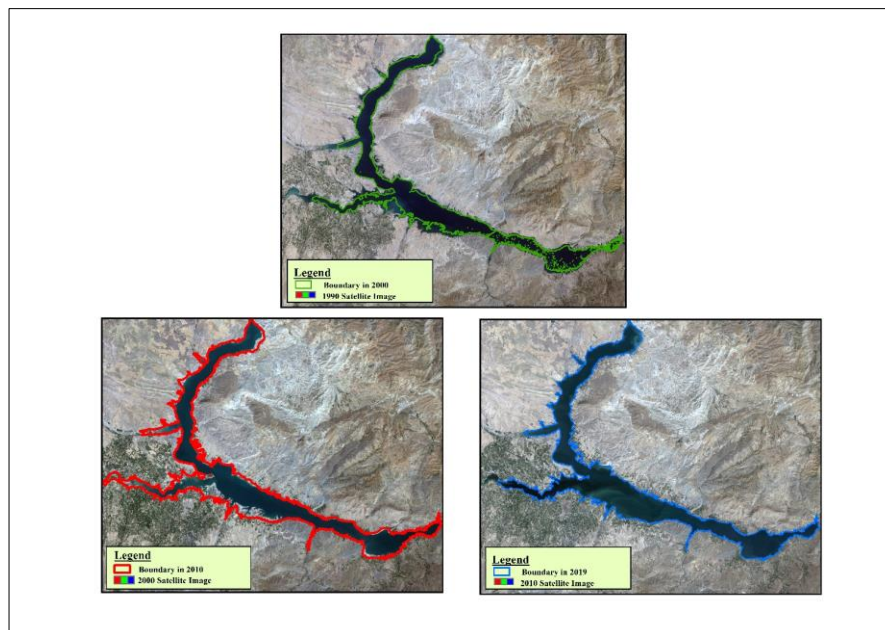


Figure 3. Produced lake boundaries - satellite image before a decade

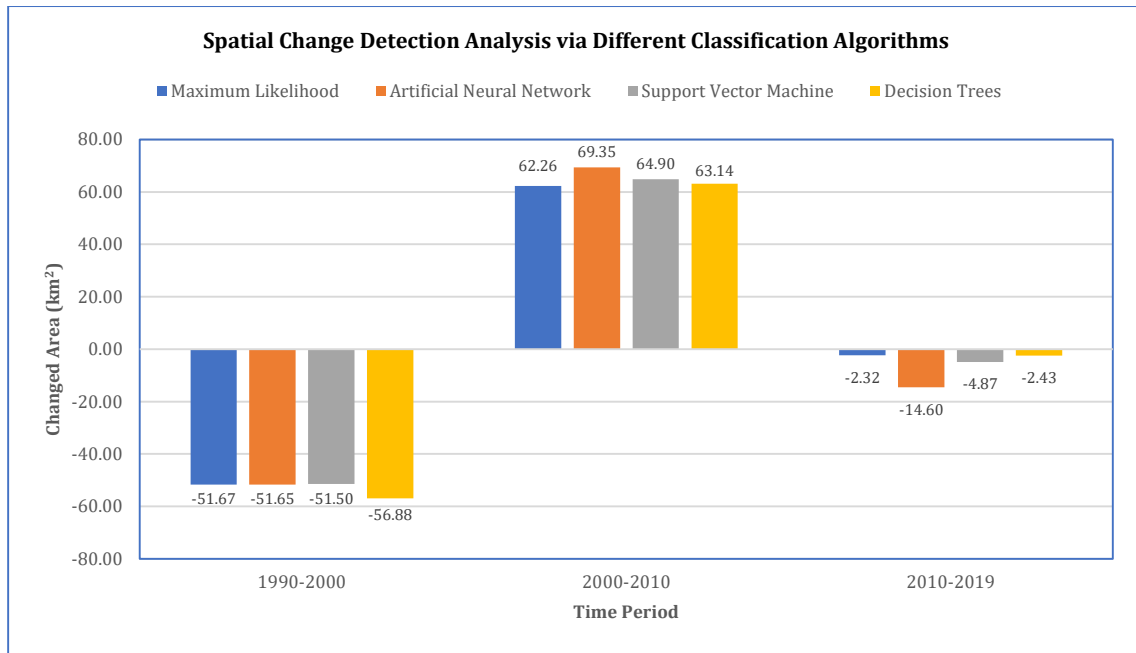


Figure 4. Spatial change detections analysis via different classification algorithms

5. DISCUSSIONS AND CONCLUSIONS

In this study, the coastline of Karakaya Dam Lake between 1990-2000-2010 and 2019 was determined by using different classification algorithms using Landsat TM, ETM and OLI images. For this purpose, thematic maps were produced and spatial change analyzes were made.

Primarily, it is understood from the sources in the article that changes in wetlands have a great connection with global climate change. While selecting the data used in this study, attention was paid to have the same seasonal data on different dates. It is thought by the authors that changes in the lake area are influenced by climatic effects as well as opening the dam covers. Different classification techniques were used in order to observe the accuracy rates during the classification processes. When the classification accuracy given in Table 2 is examined, it can be seen that the Support Vector Machines method gives the highest accuracy rate compared to other methods. The reason why each method gives different accuracy for different years is that different test data are selected for each year. Land use changes have shown that it is not appropriate to use the same test data for each year.

Water fields were separated from the classified data obtained and vector data was obtained for each year. Vector coastline produced in Figure 3 and satellite data 10 years ago are indicated by overlap. When the figure is examined, it is understood that the change that occurred between 1990 and 2000 clearly appeared. In addition, the change in water level from 2000 to 2010 is also noticeable.

If the values given in Figure 4 are examined, the data of area changes can be seen for each method. In this context, it can be said that each method gives close values for the water area. As can be seen from the chart, the negative change that occurred between

1990-2000 left its place to a positive growth between 2000-2010. However, it is understood that no major changes occurred between 2010 and 2019.

The results shown in Table 3 are based on the area designated by the General Directorate of Spatial Planning as the official coastal border. When the table is analyzed, it is seen that the difference between the classification results and official border data reached the highest point in 2000. In addition, it is observed that there was not a big change between 2010 and 2019.

In the study, the change detection analysis of Karakaya Dam Lake was made using different classification techniques. It was observed that the most influential situation on the study results was the opening times of the dam hatch fed by the lake. This dam, which was built for the first time in 1987, reached the filling level in 2004 according to official sources and the dam hatch were opened. When results analyzed, it is seen that lake water decreased in 2000 due to agricultural activities, precipitation, drought etc. In addition, during these periods of decline, old settlements, which were flooded by the lake and evacuated before the dam was built, also emerged.

This study showed how different classification algorithms affect the classification result in water areas. The accuracy of each classification algorithm used is considered to be of usable level. It is believed that new techniques and analysis that will emerge thanks to the developing and renewed technology will further strengthen the studies.

REFERENCES

Augusteijn, M. F., Warrender, C.E. (1998). Wetland classification using optical and radar data and

- neural network classification. *International Journal of remote sensing*, 19(8), 1545-1560.
- Baghdadi, N., Bernier, M., Gauthier, R., & Neeson, I. (2001). Evaluation of C-band SAR data for wetlands mapping. *International Journal of Remote Sensing*, 22(1), 71-88.
- Berberoglu, S., Yilmaz, K.T., & Ozkan, C. (2004). Mapping and monitoring of coastal wetlands of Cukurova Delta in the Eastern Mediterranean region. *Biodiversity & Conservation*, 13(3), 615-633.
- Berhane, T.M., Lane, C.R., Wu, Q., Autrey, B.C., Anenkhonov, O.A., Chepinoga, V.V., & Liu, H. (2018). Decision-tree, rule-based, and random forest classification of high-resolution multispectral imagery for wetland mapping and inventory. *Remote sensing*, 10(4), 580.
- Huang, C., Yang, L. (2001). Synergistic use of FIA data and landsat 7 ETM+ images for large area forest mapping. In *The Thirty-fifth Annual Midwest Forest Mensurationists and the Third Annual FIA Symposium*, Traverse City, MI, US.
- Ingram, J.C., Dawson, T.P., & Whittaker, R.J. (2005). Mapping tropical forest structure in southeastern Madagascar using remote sensing and artificial neural networks. *Remote Sensing of Environment*, 94(4), 491-507.
- Jensen, J.R., Qiu, F., & Ji, M. (1999). Predictive modelling of coniferous forest age using statistical and artificial neural network approaches applied to remote sensor data. *International Journal of Remote Sensing*, 20(14), 2805-2822.
- Kaplan, G., Avdan, Z. Y., & Avdan, U. (2019). Mapping and Monitoring Wetland Dynamics Using Thermal, Optical, and SAR Remote Sensing Data. *Wetlands Management: Assessing Risk and Sustainable Solutions*, 87.
- Kavzoglu, T., Colkesen, I. (2009). A kernel functions analysis for support vector machines for land cover classification. *International Journal of Applied Earth Observation and Geoinformation*, 11(5), pp.352-359.
- Kavzoglu, T., Colkesen, I. (2010). Karar ağaçları ile uydu görüntülerinin sınıflandırılması: Kocaeli örneği. *Harita Teknolojileri Elektronik Dergisi*, 2(1), 36-45.
- Lee, J. J., Shim, J. C., & Ha, Y.H. (1994). Stereo correspondence using the Hopfield neural network of a new energy function. *Pattern Recognition*, 27(11), 1513-1522.
- Lillesand, T.M., Kiefer, R.W., & Chipman, J.W. (2008). *Remote Sensing and Image Interpretation*, John Wiley & Sons, 6th Edition, New York.
- Lu, D., Weng, Q. (2007). A survey of image classification methods and techniques for improving classification performance. *International journal of Remote sensing*, 28(5), 823-870.
- Lu, S., Wu, B., Yan, N., & Wang, H. (2011). Water body mapping method with HJ-1A/B satellite imagery. *International Journal of Applied Earth Observation and Geoinformation*, 13(3), 428-434. *sensing*, 10(4), 580.
- Calò, F., Notti, D., Galve, J. P., Abdikan, S., Görüm, T., Orhan, O., Makineci H.B., Pepe A., Yakar M. & Sanli, F.B. (2018). A multi-source data approach for the investigation of land subsidence in the Konya basin, Turkey. *International Archives of the Photogrammetry, Remote Sensing and Spatial Information Sciences*, 42(3/W4).
- Colkesen, I. (2009). Uzaktan algılamada ileri sınıflandırma tekniklerinin karşılaştırılması ve analizi (Master Thesis) Gebze Technical University, Kocaeli, Turkey.
- Dean, A.M., Smith, G.M. (2003). An Evaluation of Perparcel Land Cover Mapping Using Maximum Likelihood Class Probabilities. *International Journal of Remote Sensing*, 24 (14), 2905-2920.
- Dixon, B., Candade, N. (2008). Multispectral landuse classification using neural networks and support vector machines: one or the other, or both? *International Journal of Remote Sensing*, 29(4), 1185-1206.
- Foody, G. M., Mathur, A. (2004). Toward intelligent training of supervised image classifications: directing training data acquisition for SVM classification. *Remote Sensing of Environment*, 93(1-2), 107-117.
- Foody, G.M., Arora, M.K. (1997). An evaluation of some factors affecting the accuracy of classification by an artificial neural network. *International Journal of Remote Sensing*, 18(4), 799-810.
- Foody, G.M., Mathur A. (2004). A relative evaluation of multiclass image classification by support vector machines. *IEEE Transactions on Geoscience and Remote Sensing*, 42, 1335-1343.
- Frazier, P.S., Page, K.J. (2000). Water body detection and delineation with Landsat TM data.

- Photogrammetric engineering and remote sensing, 66(12), 1461-1468.
- Fuping, G., Runsheng, W., Yongjiang, W., & Zhengwen, F. (2011). The classification method based on remote sensing techniques for land use and cover. *Remote Sensing for Land & Resources*, 11(4), 40-45.
- Ghedira, H., Bernier, M., & Ouarda, T. B. M. J. (2000). Application of neural networks for wetland classification in RADARSAT SAR imagery. In *IGARSS 2000. IEEE 2000 International Geoscience and Remote Sensing Symposium. Taking the Pulse of the Planet: The Role of Remote Sensing in Managing the Environment. Proceedings (Cat. No. 00CH37120) (Vol. 2, pp. 675-677). IEEE.*
- Goung, L., Zheng, T. (1993). Stereo matching using artificial neural networks. *International Archives of Photogrammetry and Remote Sensing*, 29, 417-417.
- Huang, C., Davis, L.S., & Townshend, J.R.G. (2002). An assessment of support vector machines for land cover classification, *International Journal of Remote Sensing*, 23(4), 725-749.
- Mather, P.M. (1987). *Computer processing of remote-sensed images.* John Wiley and Sons Ltd.
- Mathur A., Foody, G.M. (2008b). Crop classification by support vector machine with intelligently selected training data for an operational application. *International Journal of Remote Sensing*, 29, 2227-2240.
- Melgani, F., Bruzzone, L. (2004). Classification of hyperspectral remote sensing images with support vector machines. *IEEE Transactions on Geoscience and Remote Sensing*, 42, 1778-1790.
- Munyati, C. (2000). Wetland change detection on the Kafue Flats, Zambia, by classification of a multitemporal remote sensing image dataset. *International journal of remote sensing*, 21(9), 1787-1806.
- Nasr, M.S., Moustafa, M.A., Seif, H.A., & El Kobrosy, G. (2012). Application of Artificial Neural Network (ANN) for the prediction of EL-AGAMY wastewater treatment plant performance-EGYPT. *Alexandria engineering journal*, 51(1), 37-43.
- Orhan, O., Yalvac, S., & Ekercin, S. (2017). Investigation of Climate Change Impact on Salt Lake by Statistical Methods. *International Journal of Environment and Geoinformatics*, 4(1), 54-62.
- Oztemel, E. (2016). *Yapay Sinir Ağları. Papatya Yayıncılık Eğitim, İstanbul, 230 s.*
- Pal, M., Mather, P.M. (2003). An assessment of the effectiveness of decision tree methods for land cover classification. *Remote Sensing of Environment*, 86, 554-565.
- Pavuluri, M.K., Ramanathan, S., & Daniel, Z. (2002). A rule-based classifier using classification and regression tree (CART) approach for urban landscape dynamics. In *Proceedings of International Geoscience and Remote Sensing Symposium, June (pp. 24-28).*
- Pierce, L.E., Sarabandi, K., & Ulaby, F.T. (1994). Application of an artificial neural network in canopy scattering inversion. *REMOTE SENSING*, 15(16), 3263-3270.
- Pizzolato, A.N., Haertel, V. (2003). On The Application of Gabor Filtering in Supervised Image Classification, *International Journal of Remote Sensing*, 24, 2167-3189.
- Ridd, M.K., Liu, J. (1998). A comparison of four algorithms for change detection in an urban environment. *Remote sensing of environment*, 63(2), 95-100.
- Rokni, K., Ahmad, A., Selamat, A., & Hazini, S. (2014). Water feature extraction and change detection using multitemporal Landsat imagery. *Remote sensing*, 6(5), 4173-4189.
- Sahin, M. (2012). Modelling of air temperature using remote sensing and artificial neural network in Turkey. *Advances in space research*, 50(7), 973-985.
- Simard, M., Saatchi, S.S., & De Grandi, G. (2000). The use of decision tree and multiscale texture for classification of JERS-1 SAR data over tropical forest. *IEEE Transactions on Geoscience and Remote Sensing*, 38(5), 2310-2321.
- Sun, F., Sun, W., Chen, J., & Gong, P. (2012). Comparison and improvement of methods for identifying waterbodies in remotely sensed imagery. *International journal of remote sensing*, 33(21), 6854-6875.
- T.C Resmi Gazete, 20 Ocak 2013, Sayı, 4153 <https://www.resmigazete.gov.tr/eskiler/2013/01/20130120-9.htm>
- Torun, A.T. (2015). Yapay arı koloni algoritmasının tarım alanlarının sınıflandırılmasında

kullanılabilirliğinin irdelenmesi (Master thesis)
Aksaray University, Aksaray, Turkey.

Vapnik, V.N. (1995). The nature of statistical learning theory. New York, USA: Springer-Verlag.

Viotti, P., Liuti, G., & Di Genova, P. (2002). Atmospheric urban pollution: applications of an artificial neural network (ANN) to the city of Perugia. *Ecological Modelling*, 148(1), 27-46.

Walker, N.P., Eglon, S. J., & Lawrence, B.A. (1994). Image compression using neural networks. *GEC journal of research*, 11(2), 66-75.

Wei, W., Zhang, X., Chen, X., Tang, J., & Jiang, M. (2008). Wetland mapping using subpixel analysis and decision tree classification in the Yellow River delta area. In *ISPRS* (Vol. 37, pp. 667-670).

Work, E.A., Gilmer, D.S. (1976). Utilization of satellite data for inventorying prairie ponds and lakes. *Photogrammetric Engineering and Remote Sensing*, 42(5), 685-694.

Xu, M., Watanachaturaporn, P., Varshney, P.K., & Arora, M.K. (2005). Decision tree regression for soft classification of remote sensing data. *Remote Sensing of Environment*, 97(3), 322-336.

Zhang, S., Na, X., Kong, B., Wang, Z., Jiang, H., Yu, H., ... & Dale, P. (2009). Identifying wetland change in China's Sanjiang Plain using remote sensing. *Wetlands*, 29(1), 302.

Zhou, Q., Robson, M. (2001). Automated Rangeland Vegetation Cover and Density Estimation Using Ground Digital Images and a Spectral-Contextual Classifier, *International Journal of Remote Sensing*, 22 (17), 3457-3470.